Elsevier Editorial System(tm) for Soil Dynamics and Earthquake Engineering
Manuscript Draft

Manuscript Number: SOILDYN-D-16-00184R1

Title: Newmark sliding block model for predicting the seismic performance of vegetated slopes

Article Type: Research Paper

Keywords: Analytical modelling; Centrifuge modelling; Dynamics; Earthquakes; Sand; Slopes; Vegetation; Ecological Engineering

Corresponding Author: Mr. Jonathan Knappett, MA MEng PhD

Corresponding Author's Institution: University of Dundee

First Author: Teng Liang, PhD

Order of Authors: Teng Liang, PhD; Jonathan Knappett, MA MEng PhD

***Highlights (for review)**

- Newmark sliding-block procedure for slopes containing vegetation.
- Use of mobilised friction angle compatible with the strength of the input motion.
- Simulation of non-associative behaviour via an equivalent associative friction angle.
- Failure mechanism and yield acceleration from Discontinuity Layout Optimisation.
- Potential benefits of roots in reducing slip varies with the height of the slope.

Newmark sliding block model for predicting the seismic performance of vegetated slopes

T. Liang & J. A. Knappett[1]

Abstract:

This paper presents a simplified procedure for predicting the seismic slip of a vegetated slope. This is important for more precise estimation of the hazard associated with seismic landslip of naturally vegetated slopes, and also as a design tool for determining performance improvement when planting is to be used as a protective measure. The analysis procedure consists of two main components. Firstly, Discontinuity Layout Optimisation (DLO) analysis is used to determine the critical seismic slope failure mechanism and estimate the corresponding yield acceleration of a given slope. In DLO analysis, a modified rigid perfectly plastic (Mohr–Coulomb) model is employed to approximate small permanent deformations which may accrue in non-associative materials when subjected to ground motions with relatively low peak ground acceleration. The contribution of the vegetation to enhancing the yield acceleration is obtained via subtraction of the fallow slope yield acceleration. The second stage of the analysis incorporates the vegetation contribution to the slope's yield acceleration from DLO into modified limit equilibrium equations to further account for the geometric hardening of the slope under increasing soil movement. Thereby, the method can predict the permanent settlement at the crest of the slope via a slip-dependent Newmark sliding block approach. This procedure is validated against a series of centrifuge tests to be highly effective for both fallow and vegetated slopes and is subsequently used to provide further insights into the stabilising mechanisms controlling the seismic behaviour of vegetated slopes.

Key words: Analytical modelling; Centrifuge modelling; Dynamics; Earthquakes; Sand; Slopes; Vegetation; Ecological Engineering

1. Introduction

The use of vegetation to reinforce soil on landslip-prone slopes is an ecologically and economically beneficial sustainable alternative to traditional civil engineering reinforcement techniques [1-3]. The mechanical benefit of roots on slope stability has been commonly accepted. Many analytical models have been developed, based on small site in-situ investigation and laboratory tests, to quantify this benefit and predict its impacts on global slope behaviour [4-6]. However, to the best of authors' knowledge, all of these analytical models have been developed for static/monotonic use. The impacts of vegetation on seismic performance of slopes subjected to earthquake ground motions are generally overlooked in preliminary design. As observed by recent physical modelling studies [7-9], vegetation could highly improve the seismic performance of slopes (in terms of crest settlement) especially for the case of slopes of modest height (e.g. small embankments). As a result, ignoring the benefit of vegetation may lead to a conservative result and the use of more extensive remedial methods (e.g.

[1] Corresponding author: j.a.knappett@dundee.ac.uk; +44-1382-384345

piling, soil nailing) which may not be necessary. Analytical models which incorporate vegetation are therefore required for use in seismic analysis and design [10].

Eurocode 8 [11], which guides the design and construction of buildings and civil engineering works in seismic regions within Europe, recommends the use of established methods of dynamic analysis, such as Finite Elements (FE) or rigid block models or by simplified pseudo-static methods to determine the response of slopes to a design earthquake. Given the computational expense of the FE method, a complimentary simplified procedure would be highly useful in preliminary design, particularly for identifying key cases for further detailed study via FE. While compared with pseudo-static methods, Newmark sliding block models [12], which as displacement-based methods, are aligned with modern trends in performance-based design and assessment, potentially offer a useful basis for such a method, especially given their popularity. Recently, such methods have been developed to incorporate the large displacement effects of continued sliding in hardening the slope response [13], and also to incorporate the stabilising effects of a row of discretely spaced piles [14].

In this paper, an improved sliding-block procedure is developed to predict the seismic performance of vegetated slopes. The procedure consists of two components. Firstly, an analysis using Discontinuity Layout Optimisation (DLO [15]) is used to detect the critical seismic failure mechanism for slopes incorporating zones of enhanced strength where the roots are present (i.e. the lowest upper-bound mechanism using a virtual work approach and optimisation routine) and predict the contribution to the yield acceleration of a given slope configuration provided by the roots. This derived yield acceleration information is then incorporated into a modified limit equilibrium formulation for a sliding block to further account for the geometric hardening of the slope as it flattens with slip, allowing the permanent settlement at the crest of the slope to be estimated. The procedure is then validated against a database of centrifuge test results reported in [8], and subsequently used to reveal further insights into the seismic behaviour of vegetated slopes.

2. Discontinuity Layout Optimisation

2.1 Fundamental theory

Discontinuity Layout Optimisation [15] is a recently developed numerical limit analysis procedure which can be applied to a wide range of geotechnical stability problems involving cohesive and/or frictional soils. Compared with the more traditional Finite Element Limit Analysis (FELA) technique which requires discretising the problem into solid (finite) elements, DLO employs rigorous mathematical optimisation techniques to identify a critical layout of lines of discontinuity which form a kinematically-admissible collapse mechanism. These lines of discontinuity are typically ‘slip-lines’ in planar geotechnical stability problems and define the boundaries between moving rigid blocks of material which form the mechanism of collapse. Associated with this mechanism is a collapse load factor, determined via the principle of virtual work, which is an upper bound on the ‘exact’ load factor according to formal plasticity theory. The core matrix formulation for seismic problems is given in Appendix A, repeated from [16] for completeness.

2.2 Constitutive modelling of soil

DLO calculations were carried out using the software LimitState:GEO, v.2.0, which involves an adaptive solution procedure described by Gilbert & Tyas (2003) [17] to significantly reduce memory requirements and the time (of the order of a few minutes) to reach an optimised solution. The geometry of a vegetated slope problem is shown schematically in Fig.1. The root-soil matrix is modelled using smeared zones with additional representative shear strength (here incorporated into the soil behaviour as additional cohesion) reflecting the contribution of the roots, which can vary with depth. The maximum rooting depth is denoted as h_r and the lateral spread of the roots by the Critical Rooting Zone (CRZ), essentially a diameter which defines the zone of dominant structural roots which have been found to provide more than 80% of the total root mass. The two-dimensional (2D) plane strain model assumes that the input additional representative shear strength from the roots can be modelled as an equivalent amount per metre length of the slope, accounting for the plant spacing in the out-of-plane direction.

The current implementation of DLO uses a rigid-plastic material model based on the Mohr–Coulomb model with an associative flow rule for frictional materials, and this was used in the modelling presented herein. Four soil input parameters were required, namely: unit weights under saturated and dry condition and two measurable effective stress strength parameters, ϕ' and c'. Although associative flow is implicitly assumed in this model, such an assumption will overestimate the yield acceleration compared to the true non-associative behaviour in the soil due to an overestimation of the amount of dilation, and therefore potentially overestimate the yield acceleration resulting in an under-prediction of seismic slip. Hence non-associative flow should be considered pre-input [18]. As the soil model is rigid-plastic, if the strength is defined by the peak friction angle it will imply that slip will not occur until peak strength is exceeded, even though the soil may be substantially into its non-linear elasto-plastic deformation range below this level, and therefore able to accrue small permanent displacements with repetitive cyclic loading. To overcome these limitations an approximate procedure is proposed below (and validated against centrifuge data later on) to account for non-associativity and pre-peak accumulation of (small) deformations via an equivalent associative analysis with a mobilised friction angle (ϕ'_{mob}) [19] and corresponding mobilised yield acceleration for cases where the induced seismic shear stress is less than the peak shear strength of the soil to allow improved predictions of small amounts of permanent displacement in smaller earthquakes.

2.3 Influence of non-associativity

Here, non-associative flow was modelled by adjusting the value of $\phi' = \phi'_{mob}$ used in the analyses from the actual value for the true non-associative behaviour to an equivalent associative value ϕ^* as suggested in [20] and previously used for other seismic limit analysis problems (e.g.[21],[22]), given by:

$$\phi^* = \tan^{-1}\left(\frac{\cos\psi'_{mob}\sin\phi'_{mob}}{1-\sin\psi'_{mob}\sin\phi'_{mob}}\right) \quad (1)$$

where ϕ'_{mob} is a mobilised friction angle which takes a value between a lower bound of ϕ'_{cs} at critical state and an upper bound of ϕ'_{pk} if the seismically induced shear stresses would be sufficient to exceed the peak soil strength. Considering the limiting case of $\phi'_{mob} = \phi'_{pk}$, ϕ'_{pk} can be written in terms of dilation angle ψ' as:

$$\phi'_{pk} = \phi'_{cs} + 0.8\psi' \quad (2)$$

for plane strain after [23]; ϕ'_{pk} can also be given as a function of the relative dilation index I_R :

$$\phi'_{pk} - \phi_{cs} = AI_R \quad (3)$$

where A is a dimensionless factor to account for strain type (A = 5 for plane strain) and I_R is given by:

$$I_R = I_D(Q - \ln p') - R \quad (4)$$

where I_D is the relative density of the soil, Q, R are fitting parameters that depend on the intrinsic sand characteristics and p' is the mean confining stress, which can be expressed in terms of the vertical and horizontal effective stresses using:

$$p' = \frac{1}{3}(\sigma'_v + \sigma'_h) = \frac{1}{3}(\sigma'_v + 2K_0\sigma'_v) \quad (5)$$

where σ'_v is the vertical effective stress, σ'_h is the horizontal effective stress, and K_0 is the earth pressure coefficient at rest , which for normally consolidated soils may be estimated using:

$$K_0 = 1 - \sin\phi'_{cs} \quad (6)$$

Q and R can be simplified to 10 and 1 when $0 < I_R < 4$, while at very low confining stress level ($I_R > 4$), Q and R can be calculated as $7.1 + 0.75\ln p'$ (for plane strain) and 1, respectively [24].

2.4 Mobilised friction angle accounting for pre-peak deformations

The dilation angle utilised by this approach and expressed via Eq. (2) is the maximum dilation angle, corresponding to a capping yield surface. The state of soil is very strongly dependent on its stress history [25],[26] and the shape of the yield surface is determined by the maximum stress the soil has ever experienced. For smaller earthquake motions, the magnitude of the induced shear stresses may not be sufficient to push the effective stress path within the soil to the capping yield surface, though there may be accumulation of small plastic strains due to inelastic stress-strain response of the soil pre-failure. This is here represented by an expanding yield surface (described by ϕ'_{mob}) for the non-associative soil, which the induced shear stresses from

the combined effects of the ground slope and the earthquake will just reach. It is then assumed that Eq. (2) is also valid below peak strength, i.e.:

$$\phi'_{mob} = \phi'_{cs} + 0.8\psi'_{mob} \quad (7)$$

Eq. (1) is then used to approximate the non-associative values of ϕ'_{mob} and ψ'_{mob} as an equivalent associative value. When a ground motion is large enough to push the mobilised yield surface to the capping yield surface the soil will dilate to the maximum (capping) condition and any further increase in ground acceleration and seismically induced shear stress will not further change the shape of yield surface. Compared to recent previous sliding block models ([13],[22]) which considered strong ground motions with peak accelerations large enough to easily exceed the peak strength, the use of ϕ'_{mob} here extends the range of applicability to smaller ground motions, a feature which will be useful in the later validation against centrifuge data.

To incorporate the model of soil behaviour described above into a slope stability problem, it is necessary to estimate the peak induced cyclic shear stresses in the ground such that the mobilised friction angle ϕ'_{mob} can be estimated. For a slip plane at depth z beneath the slope surface (fallow soil) and parallel to it (i.e. infinite slope failure), under uniaxial horizontal shaking (i.e. plane strain – see Fig.2), the applied down slope shear stress $\tau_{applied}$ is:

$$\tau_{applied} = \gamma z \sin\beta\cos\beta + k_h \gamma z \cos^2\beta \quad (8)$$

where the first term relates to the static shear stress due to the ground slope, and the second term relates to the additional peak dynamic shear stress induced by the earthquake, (here, γ is the soil unit weight, β is the slope angle and k_h is the horizontal seismic acceleration coefficient). The effective normal stress σ' on the same slip plane is:

$$\sigma' = \gamma z \cos^2\beta - k_h \gamma z \sin\beta\cos\beta - u \quad (9)$$

where u is pore water pressure. In dry cohesionless soil, as modelled in the centrifuge testing described later, u = 0. Then the mobilised friction angle (for a cohesionless soil) may be estimated as:

$$\tan\phi'_{mob} = \frac{\tau_{applied}}{\sigma'_n} = \frac{\gamma z \sin\beta\cos\beta + k_h \gamma z \cos^2\beta}{\gamma z \cos^2\beta - k_h \gamma z \sin\beta\cos\beta} = \frac{\tan\beta + k_h}{1 - k_h \tan\beta} = \tan\left[\beta + \tan^{-1}(k_h)\right] \quad (10)$$

or alternatively,

$$\phi'_{mob} = \beta + \tan^{-1}\left(k_h\right) \quad (11)$$

Eq. (11) is applicable while $\phi'_{cs} < \phi'_{mob} < \phi'_{pk}$.

The model described in this section is shown schematically for the simplified case of c' = 0, u = 0 in Fig.3, with some indicative cyclic loading shown in the positive quadrant of a shear stress-strain plot in Fig.3 (b)-(d). The model essentially assumes that for the purposes of predicting plastic slip, a soil with a dilative peak strength

can be idealised as being elastic, accruing no plastic strain while $\phi'_{mob} < \phi'_{cs}$ (Fig.3(b)). This captures the slope being initially stable under static conditions and demonstrates that the slope can sustain a small ground motion (low k_h) without inducing slip. Once $\phi'_{mob} > \phi'_{cs}$ the model assumes that the soil will be well into its non-linear elasto-plastic range, even though $\phi'_{mob} < \phi'_{pk}$, with Eq. (11) describing the value of ϕ'_{mob} as a function of the initial slope angle (β) and the size of the earthquake shaking (k_h) (Fig.3(c)). The form of Eq. (11) implies that stronger earthquakes will induce greater slip for a given slope angle. Once $\phi'_{mob} = \phi'_{pk}$, the model reduces to a conventional slip model based on the soil initially having its peak strength. Therefore the key new feature of this model is that a low-to-moderate strength earthquake can now potentially induce some slip within a sliding block model. Previous models, even those with sophisticated strain-softening behaviour (e.g.[13][27]) required the peak strength to be exceeded before any amount of slip could take place, even if it subsequently softened rapidly to the critical state condition, and therefore could potentially predict zero slip in cases where the earthquake is moderately strong and inducing a highly non-linear elasto-plastic response within the soil. The new model therefore potentially makes sliding block analysis applicable to a wider range of earthquake motions.

2.5 Geometric-hardening and vegetation

In the forgoing section, it has been proposed that through the use of smeared zones with additional shear strength from the roots (Fig.1), and through careful selection of mobilised friction angles, DLO could be used to determine the critical failure mechanism and corresponding yield acceleration in vegetated slopes over a wide range of input motion strengths. However, one drawback of the DLO procedure (and indeed all limit analysis-type procedures for seismic problems) is that it does not immediately provide a direct measure of slope performance (e.g. seismically-induced slip) and only provides a measure of the instantaneous yield acceleration for the initial pre-earthquake slope conditions and therefore cannot account for an increase of yield acceleration due to geometric hardening of the slope with slip (defined as the benefit from the slope flattening) [13] without performing many repeat analyses on cases with reduced slope angles. In this section the sliding block method introduced by [12] and modified by [13] to allow for geometric hardening in fallow slopes is further developed to estimate the permanent deformation response of vegetated slopes, utilising only initial yield accelerations derived from DLO.

The mechanism of earthquake induced slope displacement is the sliding of an essentially rigid block (for shallow translational slips such as shown in Fig.2) along a well-defined slip surface. From Newmark's original method, sliding occurs when the shaking induced acceleration $a(t)$ exceeds the yield acceleration, k_{hy}:

$$a_{slip} = a(t) - k_{hy} \qquad (12)$$

where a_{slip} is the acceleration of the sliding mass. Those portions of the recorded acceleration that exceed the yield acceleration are integrated to obtain the cumulative displacement history of the block, *s(t)*, using the following equations:

$$v_i = \begin{cases} \int_{t_i}^{t_{i+1}} \left(a(t) - k_{hy}\right) dt, t \in [t_i, t_{i+1}] \\ 0, otherwise \end{cases} \quad (13)$$

$$d_i = \int_{t_i}^{t_{i+1}} v(t) dt, t \in [t_i, t_{i+1}] \quad (14)$$

$$s = \sum d_i \quad (15)$$

where v_i is the slip velocity in the time step t_i, d_i is an increment of slip in this time step and s is the cumulative soil slip.

Aside from the DLO approach mentioned earlier, the horizontal yield acceleration of a shallow translational slip in fallow soil may be estimated using standard limit equilibrium techniques, incorporating pseudo –static acceleration components due to the seismic ground motion, as shown previously in Fig.2 [28][29][30]. Here, the shear strength of the soil along the slip plane τ_{ult} in the fallow case, assuming that the soil failure can be described by the Mohr-Coulomb failure criterion using an equivalent associative strength parameter ϕ^*, is given by:

$$\tau_{ult} = c' + (\gamma z \cos^2 \beta - k_h \gamma z \sin \beta \cos \beta - u) \tan \phi^* \quad (16)$$

where c' is the soil cohesion (due to cementation or structure effects). The soil yields when $\tau_{applied} = \tau_{ult}$, where $\tau_{applied}$ was previously defined in Eq. (8), resulting in:

$$k_{hy(fallow)} = \frac{c' + (\gamma z \cos^2 \beta - u) \tan \phi^* - \gamma z \sin \beta \cos \beta}{\gamma z \cos^2 \beta + \gamma z \sin \beta \cos \beta \tan \phi^*} \quad (17)$$

In a vegetated slope, the mechanism is potentially more complicated given that the profile is now non-homogenous (having rooted zones and non-rooted zones of defined geometry, as shown in Fig.1). An initial assumption may be to average out the effect of the roots across the whole slope face and include it along with any true soil cohesion in the c' term in Eq. (17), that is

$$c' = c'_{soil} + \Delta\tau \quad (18)$$

where c'_{soil} is the apparent cohesion of the soil itself and $\Delta\tau$ is the additional shear strength provided by the roots. However, such an approach was used in FE simulations presented in [7] and it was found that it highly over-predicted the reinforcing effect of roots on slope performance and highly under-predicted seismically induced slip when compared to centrifuge test data. However an alternative way of expressing Eq. (17) with Eq.(18), is by dividing it into two parts, one attributed to the fallow slope and the other attributed to the mobilisation of root resistance. This gives:

$$k_{hy(rooted)} = \frac{c'_{soil} + (\gamma z \cos^2\beta - u)\tan\phi^* - \gamma z \sin\beta\cos\beta}{\gamma z \cos^2\beta + \gamma z \sin\beta\cos\beta\tan\phi^*} + \frac{\Delta\tau}{\gamma z \cos^2\beta + \gamma z \sin\beta\cos\beta\tan\phi^*} \quad (19)$$

or, alternatively:

$$k_{hy(rooted)} = k_{hy(fallow)} + \Delta k_{hy} \quad (20)$$

where Δk_{hy} is the increase of yield acceleration due to the presence of the roots. As both rooted and fallow yield accelerations can be determined using DLO, the root contribution can be estimated from:

$$\Delta k_{hy} = k^{DLO}_{hy(rooted)} - k^{DLO}_{hy(fallow)} \quad (21)$$

Eq. (20) and Eq. (21) may show small differences in the values of k_{hy} between the limit equilibrium (Eq. (20)) and DLO-derived (Eq. 21) versions depending on the appropriateness of the infinite slope limit equilibrium model for a particular slope geometry, with the DLO value more appropriately capturing the true geometry of the failure mechanism.

The slope angle will decrease with slip as crest settlements make the slope shallower (re-grading, RG). A simplified model for re-grading is shown schematically in Fig.4 after [13]. The instantaneous slope angle β_{i+1} can be estimated by the following equation,

$$\beta_{i+1} = \tan^{-1}\left(\frac{H_i - d_i \sin\beta_i}{H_i \cot\beta_i + d_i \cos\beta_i}\right) \quad (22)$$

where H_i is the height of the slope at the previous time step of the Newmark analysis. For the initial time step, $d_0 = 0$, $H_i = H$ and $\beta_i = \beta_0$ (initial slope angle). It is assumed here that once the slope has deformed to a new, smaller value of β, the failure mechanism will continue to be of the translational type, with a new slip surface parallel to the new slope surface. Then the slope angle can be re-calculated at each time step to account for the regrading of the slope based on the increment of slip occurring in the previous time step using Eq. (22). For the case of a vegetated slope, as the rooted zones are near-surface it is here assumed that they will move with the surrounding soil and that $k_{hy(rooted)}$ is affected be re-grading in the same way as $k_{hy(fallow)}$ (i.e. that the effect is related purely to the external geometry of the slope), such that Δk_{hy} in Eq. (21) will remain constant throughout the analysis. It is therefore proposed that Eq. (20) can be modified to incorporate re-grading by multiplying the $k_{hy(fallow)}$ value from DLO by a 're-grading reduction factor' determined from the limit equilibrium method without recourse to further DLO, recalculated in each time step as the slope flattens out, according to:

$$k_{hy(rooted),i} = k^{DLO}_{hy(fallow)}\left[\frac{k_{hy(fallow)}(\beta_i, \phi^*, c'_{soil}, \gamma, u_i)}{k_{hy(fallow)}(\beta_{i-1}, \phi^*, c'_{soil}, \gamma, u_{i-1})}\right] + \left(k^{DLO}_{hy(rooted)} - k^{DLO}_{hy(fallow)}\right) \quad (23)$$

with $k_{hy(fallow)}$ from Eq. (17). Eq. (23) incorporates, in an approximate way, the effects of the actual failure mechanism geometry and any changes through the addition of the roots (through the use of DLO-derived yield acceleration values), soil non-associativity (via ϕ^*) and geometric re-grading (updating of β) into a yield acceleration that can evolve as the slope slips. It requires two initial DLO analyses of the initial geometry, one

fallow and one rooted, and subsequently only Eq. (17) and Eq. (23) need to be computed at each time step within an otherwise standard Newmark sliding block analysis. A flowchart, showing the complete procedure, is shown in Fig.5. The effectiveness of this model in quantifying the performance of rooted slopes will be validated against previously reported centrifuge data [8] in the following section.

3. Validation of sliding block model

3.1 Centrifuge modelling

Dynamic centrifuge modelling was conducted using the 3.5 m diameter beam centrifuge and servo-hydraulic earthquake simulator (EQS) at the University of Dundee [31]. The modelling and observations from these tests are described in detail in [8]; only a brief summary is given here. The results of four tests from this previously reported programme are utilised herein for validation of the Newmark model, representing identical 1:2 slopes ($\beta \approx 27°$) at model scale, with varied g-level (to model slopes of different prototype height) and motion frequency content as indicated in Table 1. All values presented herein are given at prototype scale, unless specifically noted otherwise. The slope models were constructed within an Equivalent Shear Beam (ESB) container in order to replicate a semi-infinite horizontal boundary condition in the direction of shaking [32],[33]. The slopes (at model scales) were prepared using dry HST 95 silica sand at a relative density of 55%-60% to form a model slope of height 240 mm from toe to crest, with a further 80 mm underneath. Based on these dimensions, at 1:10 scale (i.e. in a 10-g test) the prototype slope was 2.4 m high from toe to crest and at 1:30 scale and 30-g, the slope was 7.2 m tall. These models are shown in Fig.6. The sand was pluviated in air around suspended model root clusters with realistic 3-D geometry that were fabricated at 1:10 and 1:30 scales using a Stratesys Inc. uPrint SE Acrylonitrile Butadiene Styrene (ABS) prototyper (also known as a 3-D printer) following the procedures outlined in [9], in each case penetrating into the slope to the same rooting depth (1.5 m). The ABS plastic root analogues were validated to be highly representative of the mechanical behaviour of real roots (in terms of Young's Modulus and tensile strength) after a series of uniaxial tension and bending tests, reported in [7],[9]. In the out-of-plane direction, model root clusters were uniformly distributed at a spacing of 1.4 m. The models were each subjected to eight successive earthquake motions, comprising three different records with distinct peak ground acceleration (PGA), duration and frequency content. The first motion (EQ1) was recorded during the 1995 Aegion earthquake (M_s 6.2) and was predicted to cause only a small amount of slip and predominantly acts to characterize the elastic dynamic behaviour of the slope. This initial motion was followed by three nominally identical stronger motions (EQ2 – EQ4) from the 1994 Northridge earthquake (M_s 6.8) and a further three (EQ5 – EQ7) from the 2009 L'Aquila earthquake (M_s 6.3), followed by a final Aegion motion (EQ8). More details about these motions can be found in [7],[8].

3.2 Determination of yield accelerations from DLO

Before the Newmark-type analysis can be conducted, yield accelerations must be determined for the fallow and rooted cases using DLO. Model layouts are shown in Fig.7 for rooted cases TL 07 (Fig.6(a)) and TL 06 (Fig.6(b)). Fallow cases had identical external geometry but without the rooted soil blocks shown in Fig.7. A

fine nodal density (1000 nodes) was used in all DLO calculations to accurately describe the geometry of the failure mechanism.

The properties of the soil within the slope were determined using the model shown in Fig.3. According to Eq. (2) to Eq. (6), peak friction angle may be evaluated as a function of depth in the two slope models shown in Fig.7 and averaged over the slope height H to obtain mean peak (upper-bound) friction angles of 47° and 44.5°, for the 2.4 m and 7.2 m slopes, respectively. Considering first the shorter slope, the recorded peak accelerations in EQ1 were 0.124g and 0.144g, for the fallow and rooted slopes, respectively, corresponding to a yield surface with an initial ϕ'_{mob} of 34° and 35°. Compared with the subsequent motions, the peak acceleration of EQ1 was relatively small. A mobilised friction angle of approximately 38° (or 38.5°) can be determined for the subsequent earthquake motions EQ2-EQ4, as shown in Fig.8 (a). Given that the peak accelerations of the remaining motions (EQ5-EQ8) are not higher than those of EQ2 to EQ4, the maximum mobilised dilation has been achieved during motion EQ2, and no further change in mobilised friction angle would be observed for the final motions. In terms of the taller slope (Fig.8 (b)) which is subject to larger motions due to the increased prototype low frequency content that could be simulated by the EQS at the higher scaling factor, the recorded peak acceleration of EQ 1 is 0.196g, which corresponds to a yield surface with an initial ϕ'_{mob} of 38°. For EQ2, the recorded peak acceleration is 0.61g, which is significantly higher than 0.31g (acceleration corresponding to the capping yield surface when $\phi'_{mob} = \phi'_{pk}$), so all subsequent motions will mobilise the full peak friction angle of the soil. These values of ϕ'_{mob} were subsequently converted to equivalent associative values ϕ^* using Eq. (1), with the values shown in Table 2.

For the rooted soil, the additional strength contribution ($\Delta\tau$) from the roots used within the smeared rooted zones (see Fig.1 & Fig.7) were input to represent the 3-D model root clusters based on the results of tests in a large direct shear apparatus (DSA) that are reported in [7] and summarised in Fig.9. In the out plane direction, the spacing between the adjacent root clusters was 1.4 m, so the input values were reduced by a factor of 1.4 compared to the measured values (this is shown in Fig.9 (b)) to determine an equivalent amount of additional shear strength in the rooted zones per metre length of the (long) slope. For future practical application in the field, $\Delta\tau$ as a function of depth could be determined using new in-situ test methods (e.g. the 'corkscrew' test) currently under development and undergoing field trials at the University of Dundee [34],[35]. The results of the DLO analyses for the different slope heights, vegetation conditions and mobilised friction angles are summarised in Table 2. In addition to the yield acceleration, the static factor of safety (F_s) is also determined in each case for context. Yield accelerations for fallow conditions were also estimated using the limit equilibrium method (Eq. 17) and these results confirm that a reasonable estimation of k_{hy} is made using DLO for the fallow cases in cohesionless soil.

The presence of roots is found to improve slope stability both in the static and dynamic condition. From Table 2, an improvement of approximately 8% and 14% is observed for the static safety factor, for the 2.4 m and 7.2 m high slopes, respectively. In the dynamic condition, the yield acceleration is increased by 14-21% and 23-39%, for the 2.4 m and 7.2 m slopes, respectively. It is clear therefore that the presence of plant roots increases slope stability and will reduce seismic slip due to increased yield acceleration.

A comparison of the failure mechanisms determined for the fallow and vegetated slopes is shown in Fig.10. It is clear that the 1:2 fallow slopes fail in a shallow translational mechanism, with a shear plane located at a depth of 0.25 m and 0.70m, for the 2.4 m and 7.2 m slopes, respectively. This is consistent with visual observations from the centrifuge tests. For the vegetated cases, different failure mechanisms are illustrated between the larger slope (7.2 m) and the smaller slope (2.4 m). For the 7.2 m high slope, the slip plane is observed to move from its fallow position at a depth of 0.7 m below the ground surface, which would have passed (at approximately mid-depth) through the rooted zone, to below the rooted zone. For the 2.4 m high rooted slope, it is subject to a much shallower (0.09m) localised slip failure between the rooted zones. This appears to be a very different 'buttressing' mechanism, similar to that identified via FE modelling of a similar slope with much simpler straight vertical rod root analogues in [7]. However, given that the roots penetrate very deeply into the 2.4m slope such that they almost touch the base of the slope (Fig. 7(a) and Fig. 10(b)), it may be that there is a deep mechanism passing beneath the roots as in the 7.2 m high slope with a similar k_{hy} that is suppressed by the closeness of the bottom boundary (as a result of the limited model container size in the centrifuge). In any case, it is apparent that the mechanism by which the roots achieve their stabilising effect is by forcing the slip plane into a less optimal position around the rooted zones, compared to the fallow case.

Historically, the contribution of roots within slope stability problems has been considered through the addition of $\Delta\tau$ along the unaltered fallow position of the slip plane, i.e. an increase of strength, rather than a change in mechanism. This would previously have suggested that in order to maximise the effect of the vegetation, species should be selected to have a large root area ratio and the strongest biomechanical strength (i.e. lots of strong roots). The results shown here suggest that knowing the root shear strength contribution is still important, but that (i) it is important to understand how this varies with position (particularly depth) in the soil, rather than just conducting shear box tests of rooted soil block samples at a single depth, as this will affect the optimal position of the shear plane as found using DLO; and (ii) once the roots provide a strong enough contribution to force the slip plane to pass beneath them, there will be little point in targeting further root strength. This suggests that if planting vegetation to improve slope performance, it may not be ideal to limit species choice to the strongest rooting species, but that selection should be made based on rooting depth (and, potentially, lateral root spread, CRZ) to result in the greatest deviation in the position of the slip plane. This will be explored further in a later section.

3.3 Prediction of slip via sliding block analyses

Sliding-block analyses were subsequently conducted for each of the centrifuge tests, for the complete set of eight successive earthquake motions. The input earthquake motion used was the acceleration record measured at instrument ACC2 in each case (Fig. 6). The effects of root resistance, geometric re-grading (change in β) and non-associativity on the yield acceleration compared to the fallow slope using the mobilised friction angles for EQ1(small earthquake) and EQ2 (large earthquake) of TL 06 is shown in Fig. 11 as an example. Only the positive (downslope) accelerations have been shown for clarity. For the dry, cohesionless soil used in the centrifuge tests, Eqs. (17) and (23) become:

$$k_{hy(fallow),i} = \frac{\tan\phi^* - \tan\beta_i}{1+\tan\beta_i \tan\phi^*} \qquad (24)$$

$$k_{hy(rooted),i} = k^{DLO}_{hy(fallow)} \left[\frac{\left(\tan\phi^* - \tan\beta_i\right)\left(1+\tan\beta_{i-1}\tan\phi^*\right)}{\left(1+\tan\beta_i\tan\phi^*\right)\left(\tan\phi^* - \tan\beta_{i-1}\right)} \right] + \left(k^{DLO}_{hy(rooted)} - k^{DLO}_{hy(fallow)}\right) \qquad (25)$$

It can be seen that the model considering non-associativity via ϕ^* increases the initial yield acceleration compared with an analysis using a critical state strength model (strain hardening, SH, to ϕ'_{cs}). As a result, a large portion of EQ1 is below the yield acceleration and this will strongly influence the deformation response (this will be illustrated later). It is worth noting here that the effect of root resistance on yield acceleration was constant between EQ1 and EQ2. This is clearly a simplification of the problem because in reality, root resistance will be mobilised progressively with slip rather than instantaneously reaching peak resistance. However, given that root-soil interaction will mobilise very rapidly with slip due to the small diameter of the roots [7], this simplification is considered to be a reasonable approximation in an analysis which is designed to be practical to use. Geometric re-grading causes the yield acceleration to increase non-linearly throughout the earthquake with continuing slip (this is most noticeable for the larger motion, EQ2, in Fig.11 (b)), which will lead to reduced slip velocity and hence reduced permanent slip compared with the case with no geometric hardening.

3.4 Fallow slopes

Fig.12 and Fig.13 show the cumulative crest settlement across the eight earthquakes as predicted by the new sliding block model and compare these predictions to the values measured in the centrifuge tests, for the 1:30 scale (7.2 m high) slope and the 1:10 scale (2.4 m high) models, respectively. In Fig.12, predictions are made based on both Eq. (17), which uses ϕ^* based on ϕ'_{mob}, and also using a previous strain-softening model [13]. As the earthquake motions were large enough to mobilise ϕ'_{pk} in all but EQ1, this case is a test of the suitability of using ϕ^* within analyses; this is shown to give a very good match to the centrifuge data. In terms of the 2.4 m slope, because of the smaller motions in this test, all of the earthquakes have $\phi'_{mob} < \phi'_{pk}$, so this represents a good test of the new sub-peak slip model (Eq. 11). As the earthquake motions get stronger, the mobilised friction angle increases from 34° to 36.7°and 38°, for EQ1, EQ2 and the last six motions, respectively. The match to the centrifuge data is very good, with the new model capturing the accrual of small deformations (of the order of ~40 mm total, compared to the ~300 mm in Fig. 12). In contrast, the use of the previous model from [13] predicts no slip in the 2.4 m case, as despite having a sophisticated strain-softening model, the dynamically-induced shear stresses are never sufficient to exceed the peak strength and thereby trigger slip.

3.5 Rooted slopes

Fig.14 shows the results of simulations of cumulative crest displacement compared with the centrifuge test data, for the 7.2 m rooted slope. A good match to the total measured crest settlement at the end of the test is presented. A reduction of 15% in calculated permanent crest settlement is observed compared to the fallow case through the modified sliding block model results. This reduction is consistent with the reduction in slip observed in the centrifuge tests (15%). The sliding block model does not quite capture the reduction within each motion

perfectly – as observed, the root contribution is mainly mobilised in EQ4 in the centrifuge tests, but this is mobilised from EQ2 progressively in the simulated case.

Results for the 2.4 m rooted slope case are presented in Fig.15. Here, four cases were considered: case (a) is a direct comparison to the fallow case, with the only difference being the addition of the rooted zones; case (b) is established to account for the root buttressing behaviour observed in DLO (Fig. 7(a)), and is achieved by adjusting the slope height from 2.4m to 0.4 m in the calculation; case (c) corresponds to the reduction of peak acceleration observed in centrifuge tests (by 10% - 20% at instruments ACC 6, 7, 10 and 11 in Fig.6 (a)) due to the presence of the roots in this particular test and is incorporated by multiplying the input motion by a factor of 0.85 to obtain a new input motion [9]; case (d) considers the combined effects of case (b) and case (c). It can clearly be seen that case (a) without consideration of the acceleration reduction effect highly under-estimates the contribution of the roots in reducing the slope crest deformation response. Compared to the fallow case, the inclusion of roots (case (a)) reduced the crest settlement by 61%; accounting for the buttressing effect (case (b)) reduced it by 74%; the reduction in acceleration (case (c)) reduces it by 86% and the combined effects (case (d)) result in a reduction of 89%, which is a little higher than the reduction observed in the centrifuge tests (85%). The reason for this is associated with the fact that the contribution of roots is mainly mobilized during the first two motions and then has an apparently less significant effect for the last six motions in the centrifuge tests but the simulated case assumes that the root contribution remains constant across the eight earthquakes. Fig.15 suggests that the contribution of roots to reducing seismic slip within slopes is a combination of an increase in yield acceleration associated with a change of failure mechanism and a small reduction in accelerations within the slipping mass. Fig.16 summarises the results of all of the predictions at the end of each earthquake motion, from which it can be seen that the new model is effective across the full range of slope heights and motions tested, for both fallow and rooted slopes.

4. Further insights into rooted slope seismic behaviour

In this section, the influence of the root contribution to shear strength is further investigated using the modified sliding-block procedure, particularly to explore the aforementioned feature of the increase in yield acceleration and reduction in slip resulting principally from a change in mechanism rather than the addition of root strength along the fallow slip plane. Starting with the $\Delta\tau$-depth profiles shown in Fig.9, the values of $\Delta\tau$ were progressively reduced at all depths by a constant factor. This could represent the use of a different species which has a smaller strength contribution (but similar distribution with depth), or a slope with the initial strength distribution considered herein as the vegetation dies and the roots subsequently decay. The variation of yield acceleration with the reduction of root cohesion as determined from DLO is shown in Fig.17 (a). The normalised root contribution is the reduction factor used to multiply the initial $\Delta\tau$-depth profile (essentially the percentage strength remaining if the roots were decaying); the normalised yield acceleration is $k_{hy(rooted)}$ from DLO, divided by $k_{hy(fallow)}$, also from DLO. Fig.17 (b) shows crest settlements subsequently computed using the Newmark procedure, where the normalised settlement is the crest settlement of the rooted case divided by the crest settlement of the fallow case. Mechanisms for some of the key low strength cases showing transitions in behaviour are given in Fig.18. It can be seen that the yield acceleration remains constant even when the

normalised root contribution decreases to 2.5% of its initial strength for the 2.4 m slope (0.4-0.5 kPa of normalised root contribution within the rooted zone). FE model simulations reported in [36] show almost identical reinforcing effect at 100% normalised root contribution, and also suggest that the reinforcing effect can be maintained down to 25% of the initial value of the normalised root contribution (i.e. over a wide range of $\Delta\tau$ values) in the 2.4 m case – Fig.18 (b). However a smoother transition to no effect at zero normalised root contribution is shown in the FE compared to the more abrupt change in the approximate DLO-Newmark approach. For the taller slope, there is again a very close match to FE simulations at 100% normalised root contribution. The reduction in yield acceleration as the normalised root contribution is reduced is more sudden for the DLO-Newmark approach in this case reducing once normalised root contribution becomes less than 7.5%. The FE simulations again show a more progressive reduction in reinforcing effect compared to the DLO-Newmark approach. However, it is clear in both cases that (i) a substantial component of the reinforcing effect of the roots can be maintained even if the root contribution is only half as strong, which has important implications for vegetation management in allowing new vegetation to establish as older roots decay; and (ii) once the failure mechanism has moved deeper, there is no further increase in yield acceleration with stronger roots, which suggests that for the use of vegetation in engineering practice, species should be selected on the basis of maximum h_r (and CRZ) to alter the failure mechanism as much as possible, rather than selecting for the strongest possible roots.

5. Conclusions

An improved Newmark sliding-block procedure, which can include the effect of plant roots on seismic slope performance, has been developed and validated against dynamic centrifuge data. The procedure consists of two components. Firstly, DLO analysis is used to determine the seismic slope failure mechanism and estimate the corresponding yield accelerations of a given slope in fallow and rooted cases. A rigid perfectly plastic (Mohr–Coulomb) model with associative flow is used to model the soil, but utilises mobilised equivalent friction angles to approximate both the non-associative behaviour of cohesionless slopes and predict small accrued deformations when the earthquake-induced shear stresses are not sufficient to exceed peak strength, but may result in non-linear elasto-plastic behaviour and some plastic straining. The second stage utilises these derived yield accelerations from DLO into a modified Newmark sliding block approach to predict the permanent settlement at the crest of the slope; this also accounts for the geometric hardening (flattening) of the slope with continued slip making the model suitable for whole-life performance estimation. This procedure has been validated to be highly effective in predicting permanent slip for both fallow and vegetated slopes as measured in centrifuge tests and can be easily performed in preliminary design with lower computational effort than Finite Element modelling. Some factors that may influence the seismic performance of root reinforced slopes were also revealed during the development of sliding-block model. The presence of roots increase the slip plane depth and it is this effect which is principally responsible for increasing the yield acceleration and hence reducing deformations within the slope. This is in contrast to previous models which assume roots add additional shear strength onto the pre-existing (fallow) shear plane. This new finding suggests that once the roots provide enough additional shear strength to deviate the shear plane in this manner, the key controlling property of the roots will

be the rooting depth (and possibly also spread) rather than the strength of the roots. The potential benefit of roots appears to vary with the size of the slope. For taller slopes where the root depth is only a small proportion of the slope height (low h_r/H), roots only increase the yield acceleration of the slope against dynamic loading. For smaller slopes with higher h_r/H the proportional effect of this increase in yield acceleration appears to be more significant, and there is some evidence that the roots also reduce the strength of the earthquake motion within the slipping mass resulting in increased effectiveness and much reduced deformation response at the crest. Vegetation may therefore be particularly effective in smaller slopes, offering a low cost and low carbon alternative that could potentially replace more traditional stabilisation methods.

Appendix A

This appendix is from [16]. The primal kinematic problem formulation for the plane strain analysis of a quasi-statically loaded, perfectly plastic cohesive-frictional body discretised using m nodal connections (slip-line discontinuities), n nodes and a single load case can be given by

$$\min \lambda \mathbf{f}_L^T \mathbf{d} = -\mathbf{f}_D^T \mathbf{d} + \mathbf{g}^T \mathbf{p} \qquad \textbf{(A.1)}$$

subject to

$$\mathbf{B}\mathbf{d} = \mathbf{0} \qquad \textbf{(A.2)}$$

$$\mathbf{N}\mathbf{p} - \mathbf{d} = \mathbf{0} \qquad \textbf{(A.3)}$$

$$\mathbf{f}_L^T \mathbf{d} = 1 \qquad \textbf{(A.4)}$$

$$\mathbf{p} \geq \mathbf{0} \qquad \textbf{(A.5)}$$

where $\mathbf{f}_D$ and $\mathbf{f}_L$ are vectors containing respectively specified dead and live loads, $\mathbf{d}$ contains displacements along the discontinuities, where $\mathbf{d}^T = \{s_1, n_1, s_2, n_2, \cdots, n_m\}$ and s_i and n_i are the relative shear and normal displacements between blocks at discontinuity i; $\mathbf{d}^T = \{c_1 l_1, c_2 l_2, \cdots, c_m l_m\}$, where l_i and c_i are respectively the length and cohesive shear strength of discontinuity i. $\mathbf{B}$ is a suitable ($2n \times 2m$) compatibility matrix , $\mathbf{N}$ is a suitable ($2m \times 2m$) flow matrix and $\mathbf{p}$ is a ($2m$) vector of plastic multipliers. The discontinuity displacement in $\mathbf{d}$ and the plastic multipliers in $\mathbf{p}$ are the linear programing variables.

For seismic problems, pseudo-static theory may be employed [16]. The imposition of horizontal and vertical seismic acceleration within the system results in additional work terms in the governing equation that are analogous to that for self- weight. Here, the contribution made by discontinuity i to the $\mathbf{f}_D^T \mathbf{d}$ term in Eq. (A.1) can be written as

$$\mathbf{f}_{Di}^{T}\mathbf{d}_i = \left\{(1-k_v)\begin{bmatrix}-W_i\chi_i & -W_i\alpha_i\end{bmatrix} + k_h\begin{bmatrix}-W_i\alpha_i & W_i\chi_i\end{bmatrix}\right\}\begin{bmatrix}s_i\\ n_i\end{bmatrix} \quad \textbf{(A.6)}$$

where k_v and k_h are the vertical and horizontal pseudo-static acceleration coefficients, respectively; W_i is the total weight of the strip of material laying vertically above discontinuity *i*; α_i and χ_i are the horizontal and vertical direction cosines of the discontinuity in question.

The DLO method finds the optimal collapse mechanism for the problem studied. This is achieved through increasing loading within the system until collapse is achieved, by applying what is termed an 'adequacy factor' to a given load. In the case of seismic loading, this factor is applied to the horizontal or vertical acceleration. To apply live loading to the horizontal and vertical acceleration, the $\mathbf{f}_D^T\mathbf{d}$ term in Eq. (A.1) is not modified, instead modification is performed on the $\mathbf{f}_L^T\mathbf{d}$ terms, and given by

$$\mathbf{f}_{Li}^{T}\mathbf{d}_i = \left\{k_v\begin{bmatrix}-W_i\beta_i & -W_i\alpha_i\end{bmatrix} + k_h\begin{bmatrix}-W_i\alpha_i & W_i\beta_i\end{bmatrix}\right\}\begin{bmatrix}s_i\\ n_i\end{bmatrix} \quad \textbf{(A.7)}$$

Acknowledgements

The authors would like to express their sincere gratitude to Mark Truswell, Colin Stark and Gary Callon at the University of Dundee for their assistance in printing the model root analogues and undertaking the centrifuge test programme. The first author would like to acknowledge the financial support of the China Scholarship Council.

References

[1] Coppion NJ, Richards IG. Use of vegetation in civil engineering. CIRIA, London, UK; 1990.

[2] Norris JE, Stokes A, Mickovski SB, Cammeraat E, Van Beek R, Nicoll BC, et al. Slope stability and erosion control: Ecotechnological solutions. Springer, Netherlands; 2008. doi:10.1007/978-1-4020-6676-4.

[3] Stokes A, Douglas GB, Fourcaud T, Giadrossich F, Gillies C, Hubble T, et al. Ecological mitigation of hillslope instability: Ten key issues facing researchers and practitioners. Plant Soil 2014;377:1–23. doi:10.1007/s11104-014-2044-6.

[4] Wu TH. Investigation of Landslides on Prince of Wales Island, Alaska. Geotech Eng Rep 5 Civ Eng Dep Ohio State Univ Columbus, Ohio, USA 1976.

[5] Greenwood JR, Norris JE, Wint J. Assessing the contribution of vegetation to slope stability. Proc ICE - Geotech Eng 2004;157:199–207. doi:10.1680/geng.2004.157.4.199.

[6] Wu TH. Root reinforcement of soil: review of analytical models, test results, and applications to design. Can Geotech J 2013;50:259–74.

[7] Liang T, Knappett JA, Duckett N. Modelling the seismic performance of rooted slopes from individual root–soil interaction to global slope behaviour. Géotechnique 2015;65:1–15. doi:10.1680/jgeot.14.P.207.

[8] Liang T, Knappett JA. Centrifuge modelling of the influence of slope height on the seismic performance of rooted slopes. Géotechnique 2017:In Press. doi:http://dx.doi.org/10.1680/jgeot.16.P.072.

[9] Liang T, Knappett JA, Bengough AG, Ke YX. Small scale modelling of plant root systems using 3-D printing , with applications to investigate the role of vegetation on earthquake induced landslides. Landslides 2017. doi:10.1007/s10346-017-0802-2.

[10] Hess DM, Leshchinsky BA, Bunn M, Benjamin Mason H, Olsen MJ. A simplified three-dimensional shallow landslide susceptibility framework considering topography and seismicity. Landslides 2017. doi:10.1007/s10346-017-0810-2.

[11] BSI. Eurocode 8: Design of stuctures for earthquake resistance -part 5: Foundations,retaining strctures and geotechincal aspects, EN 1998-5:2004. Bristish Standard Institution, UK, 2005.

[12] Newmark NM. Effects of Earthquakes on Dams and Embankments. Géotechnique 1965;15:159–60. doi:10.1680/geot.1965.15.2.139.

[13] Al-Defae AH, Caucis K, Knappett JA. Aftershocks and the whole-life seismic performance of granular slopes. Géotechnique 2013;63:1230–44. doi:10.1680/geot.12.P.149.

[14] Al-Defae AH, Knappett JA. Centrifuge Modeling of the Seismic Performance of Pile-Reinforced Slopes. J Geotech Geoenvironmental Eng 2014;140:1–13. doi:10.1061/(ASCE)GT.1943-5606.0001105.

[15] Smith C, Gilbert M. Application of discontinuity layout optimization to plane plasticity problems. Proc. R. Soc., 2007, p. 2461–84. doi:10.1098/rspa.2006.1788.

[16] Smith CC, Cubrinovski M. Pseudo-static limit analysis by discontinuity layout optimization: Application to seismic analysis of retaining walls. Soil Dyn Earthq Eng 2011;31:1311–23. doi:10.1016/j.soildyn.2011.03.014.

[17] Gilbert M, Tyas A. Layout optimization of large-scale pin-jointed frames. Eng Comput 2003;20:1044–64.

[18] Michalowski R, Shi L. Bearing capacity of footings over two-layer foundation soils. J Geotech Eng 1995;3:421–8.

[19] Bolton MD, Take WA. Seasonal ratcheting and softening in clay slopes, leading to first-time failure. Géotechnique 2011;61:757–69. doi:10.1680/geot.9.P.125.

552 [20] Detournay E, Drescher A. Limit load in translational failure mechanisms for associative and non-
553 associative materials. Géotechnique 1993;43:443–56. doi:10.1680/geot.1993.43.3.443.

554 [21] Knappett JA, Haigh SK, Madabhushi SPG. Mechanisms of failure for shallow foundations under
555 earthquake loading. Soil Dyn Earthq Eng 2006;26:91–102. doi:10.1016/j.soildyn.2004.11.021.

556 [22] Al-Defae AH, Knappett JA. Newmark sliding block model for pile-reinforced slopes under earthquake
557 loading. Soil Dyn Earthq Eng 2015;75:265–78. doi:10.1016/j.soildyn.2015.04.013.

558 [23] Bolton MD. The strength and dilatancy of sands. Géotechnique 1986;36:65–78.
559 doi:10.1680/geot.1986.36.1.65.

560 [24] Chakraborty T, Salgado R. Dilatancy and Shear Strength of Sand at Low Confining Pressures. J
561 Geotech Geoenvironmental Eng 2010;136:527–32. doi:10.1061/(ASCE)GT.1943-5606.0000237.

562 [25] Schofield AN, Wroth CP. Critical state soil mechanics. 1968.

563 [26] Wood DM. Soil Behaviout and Critical State Soil Mechanics. Cambridge Univ Press 1990.

564 [27] Matasovic, N.Jr., Kavazanjian E. Newmark deformation analysis with degrading yield acceleration.
565 Procedings Geosynth. Long Beach, CA, USA, vol. 2, 1997, p. 989–1000.

566 [28] Sarma SK. Stability analysis of embankments and slopes. Géotechnique 1973;23:423–33.
567 doi:10.1680/geot.1973.23.3.423.

568 [29] Bray JD, Rathje EM. Earthquake-Induced Displacements of Solid-Waste Landfills. J Geotech
569 Geoenvironmental Eng 1998;124:242–53. doi:10.1061/(ASCE)1090-0241(1998)124:3(242).

570 [30] Bray JD, Travasarou T. Simplified Procedure for Estimating Earthquake-Induced Deviatoric Slope
571 Displacements. J Geotech Geoenvironmental Eng 2007;133:381–92. doi:10.1061/(ASCE)1090-
572 0241(2007)133:4(381).

573 [31] Brennan AJ, Knappett JA, Loli M, Anastasopoulos I, Brown MJ. Dynamic centrifuge modelling
574 facilities at the University of Dundee and their application to studying seismic case histories. Proc. 8th
575 Int. Conf. Phys. Model. Geotech. Perth, Aust., vol. 1, 2014, p. 227–33.

576 [32] Zeng X, Schofield AN. Design and performance of an equivalent-shear-beam container for earthquake
577 centrifuge modelling. Géotechnique 1996;46:83–102. doi:10.1680/geot.1996.46.1.83.

578 [33] Madabhushi SPG, Teymur B. Experimental study of boundary effects in dynamic centrifuge modelling.
579 Géotechnique 2003;53:655–63. doi:10.1680/geot.2003.53.7.655.

580 [34] Meijer GJ, Bengough AG, Knappett JA, Loades KW, Nicoll BC. New in situ techniques for measuring
581 the properties of root-reinforced soil – laboratory evaluation. Geotechnique 2016;66:27–40.
582 doi:http://dx.doi.org/10.1680/jgeot.15.P.060.

583 [35] Meijer G, Bengough A, Knappett JA, Loades KW, Nicoll BC. Comparison of new in situ root-
584 reinforcement measuring devices to existing techniques. Proc. XVI Eur. Conf. Soil Mech. Geotech. Eng.
585 Edinburgh, Inst. Civ. Eng., 2015, p. 1621–6. doi:10.1680/ecsmge.60678.vol4.239.

586 [36] Liang T. Seismic performance of vegetated slopes. PhD thesis,University of Dundee,UK, 2015.

587

All tables

Table 1. Summary of centrifuge models tested

Test identification number	Scale	Slope height (m)	Rooting type	Root cluster quantity	Plant spacing, out-of-plane (m)	Motion frequency content (Hz)
TL 04	1:10	2.4	Fallow	0	/	4-30
TL 05	1:30	7.2	Fallow	0	/	1.33-10
TL 06	1:30	7.2	1:30 scale root cluster	36	1.4	1.33-10
TL 07	1:10	2.4	1:10 scale root cluster	4	1.4	4-30

Table 2. Static and dynamic slope stability data

Model ID	Slope type	Slope height (m)	Motion	ϕ'_{mob}	ϕ^*	F_s (DLO)	z_{silp} (m)	k_{hy} (DLO)
DLO 01	Fallow	2.4	EQ1	34°	29.8°	1.246	0.36	0.057g
DLO 02	Fallow	2.4	EQ2-EQ8	38°	33.6°	1.435	0.25	0.124g
DLO 03	Fallow	2.4	EQ1	35°	30.7°	1.289	0.36	0.073g
DLO 04	Rooted	2.4	EQ1	35°	30.7°	1.399	0.20*	0.089g
DLO 05	Fallow	2.4	EQ2-EQ8	38.5°	34.0°	1.456	0.25	0.132g
DLO 06	Rooted	2.4	EQ2-EQ8	38.5°	34.0°	1.574	0.20*	0.151g
DLO 07	Fallow	7.2	EQ1	38°	33.6°	1.382	0.75	0.125g
DLO 08	Rooted	7.2	EQ1	38°	33.6°	1.58	1.50	0.174g
DLO 09	Fallow	7.2	EQ2-EQ8	44.5°	39.8°	1.724	0.50	0.238g
DLO 10	Rooted	7.2	EQ2-EQ8	44.5°	39.8°	1.976	1.50	0.293g

* These cases showed a local slip between root clusters (buttressing effect of roots – Fig.8)

Figure 1

Click here to download high resolution image

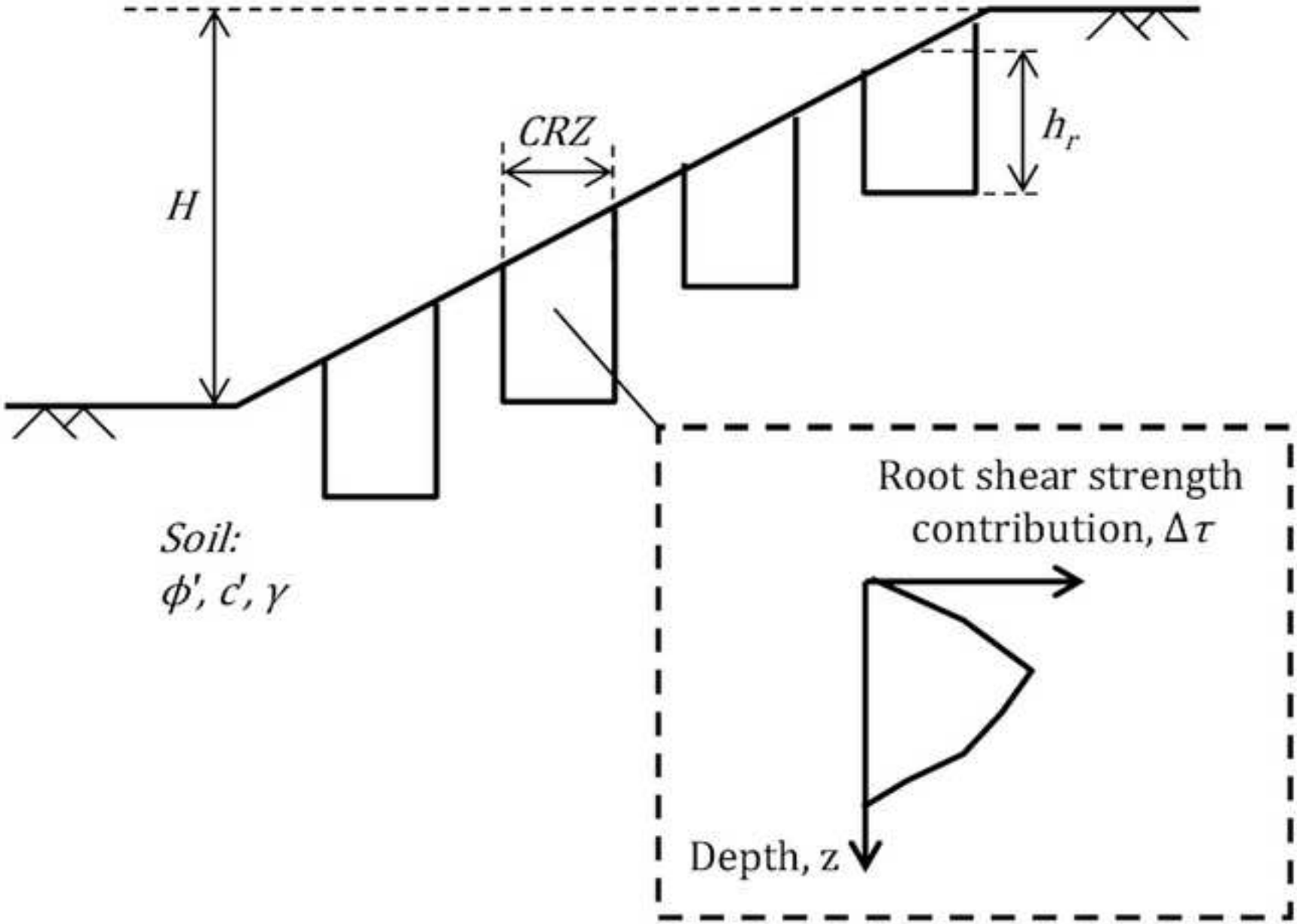

Figure 2

Click here to download high resolution image

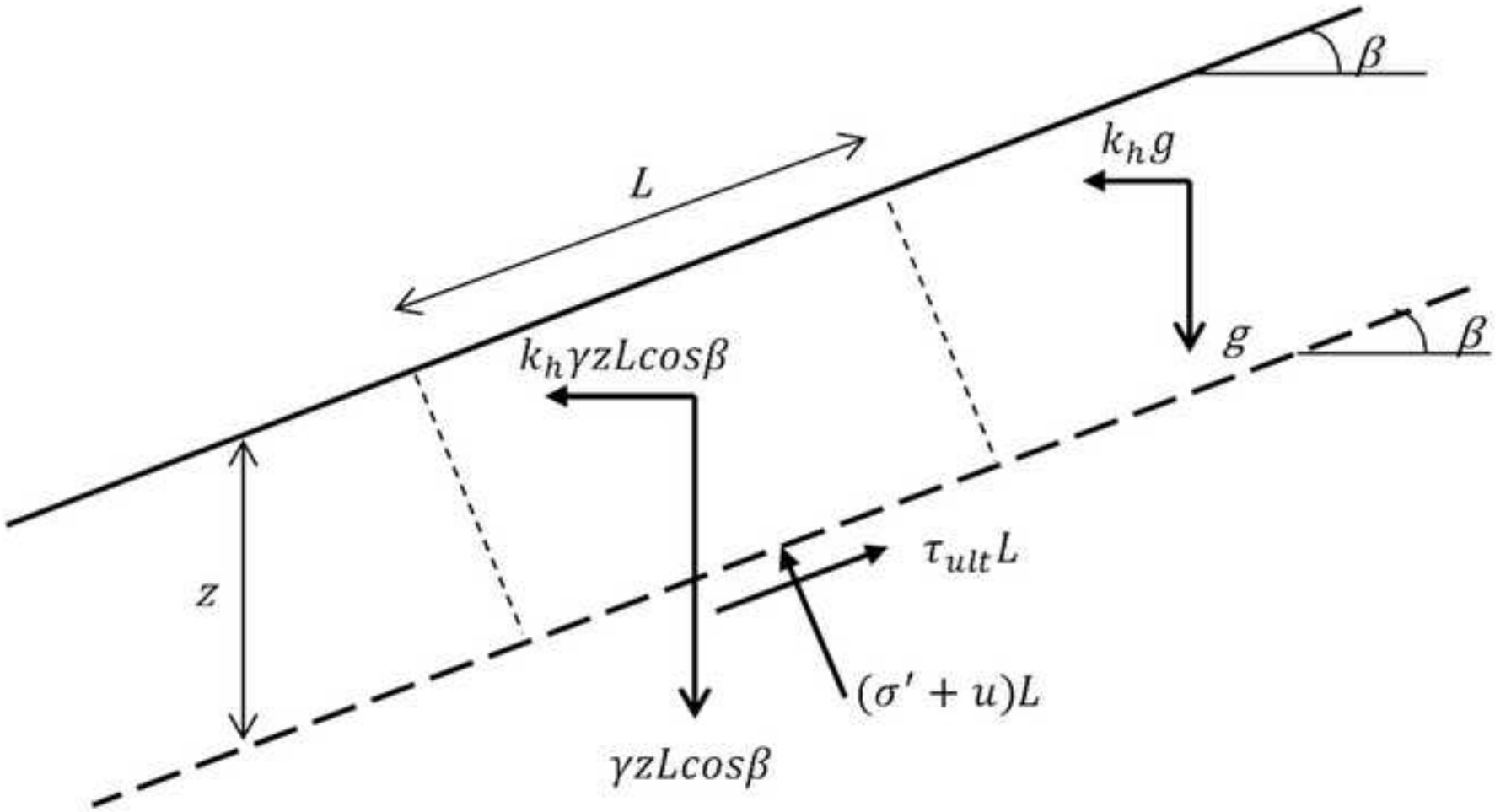

Figure 3

Click here to download high resolution image

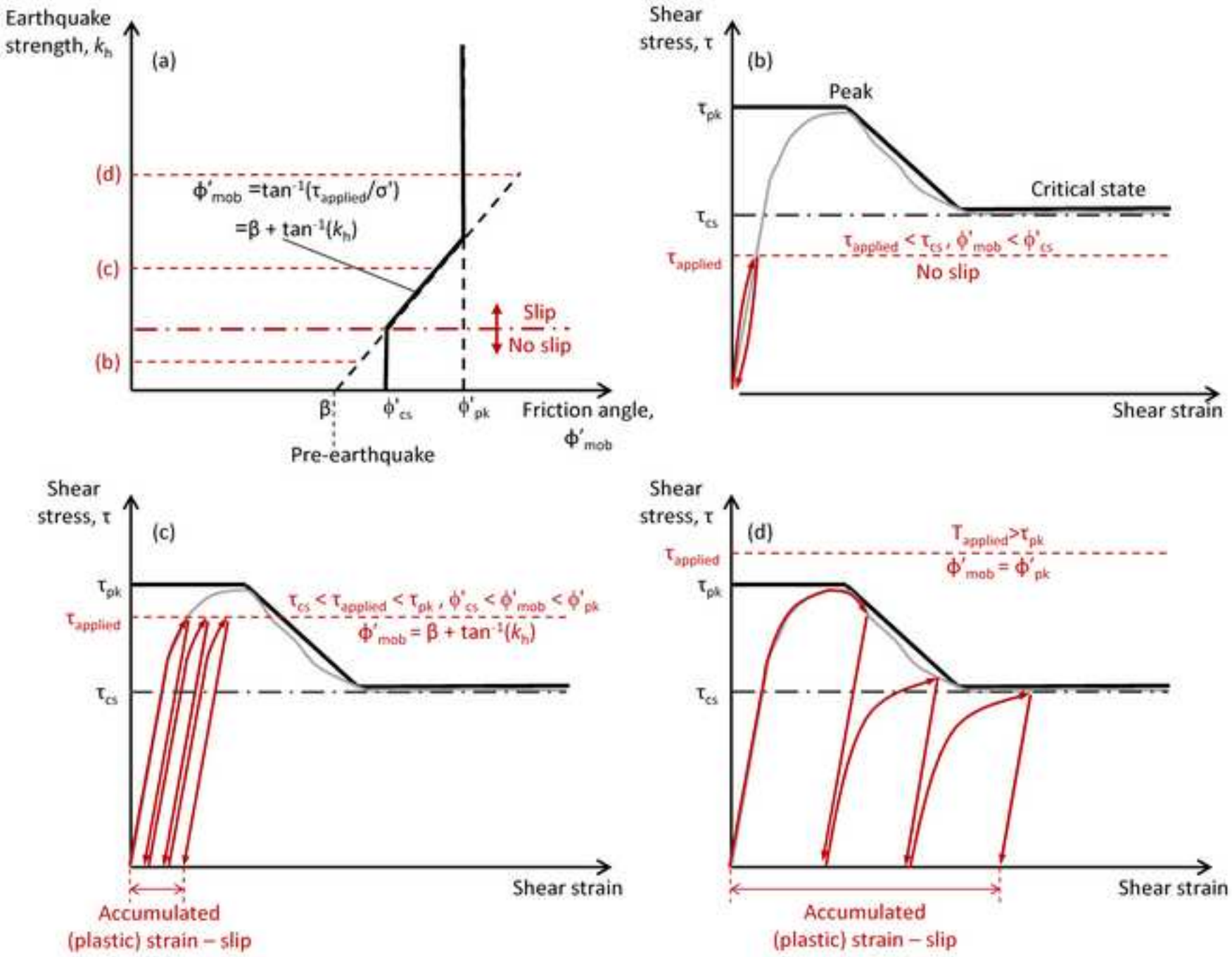

Figure 4

Click here to download high resolution image

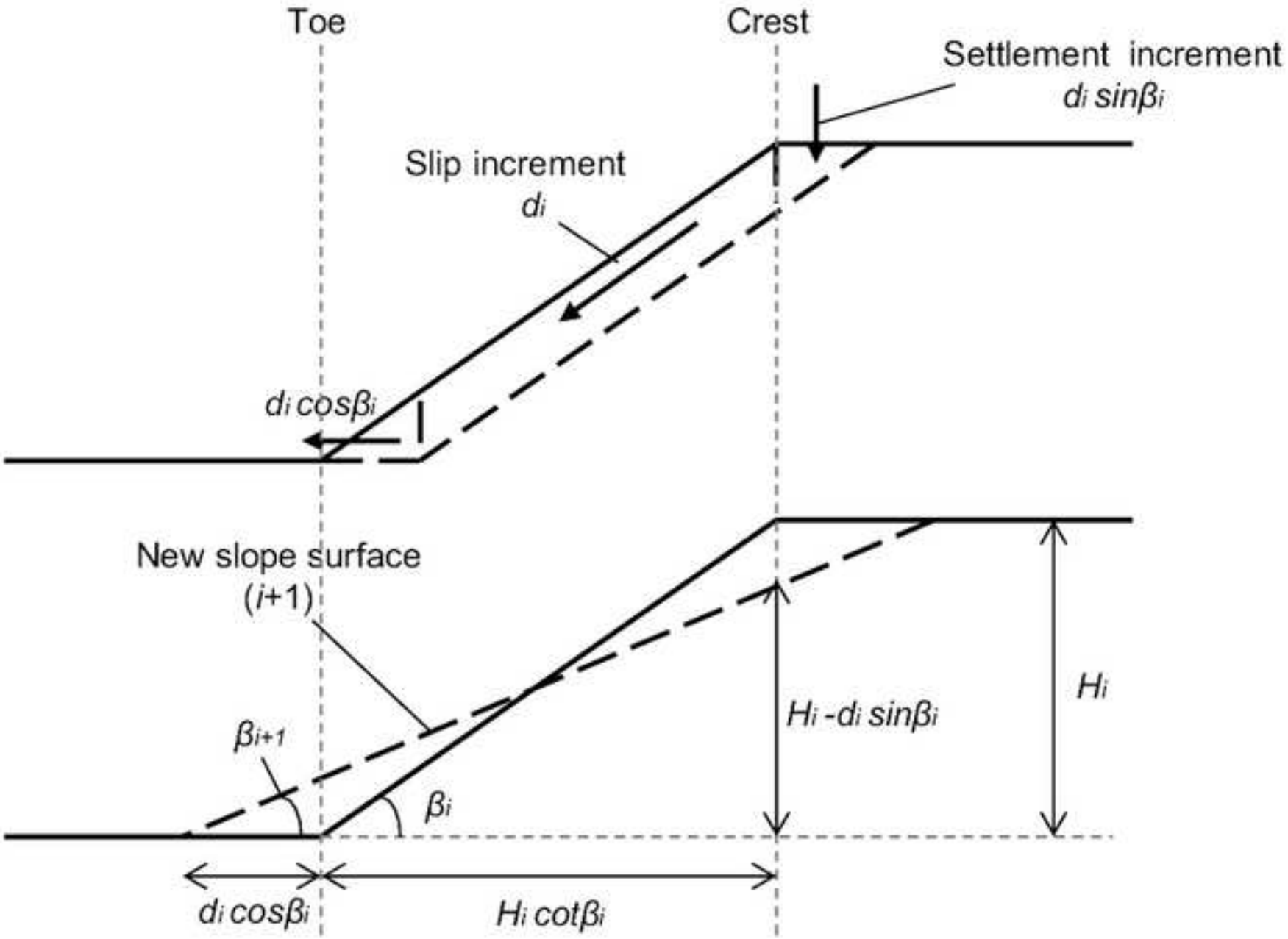

Figure 5

Click here to download high resolution image

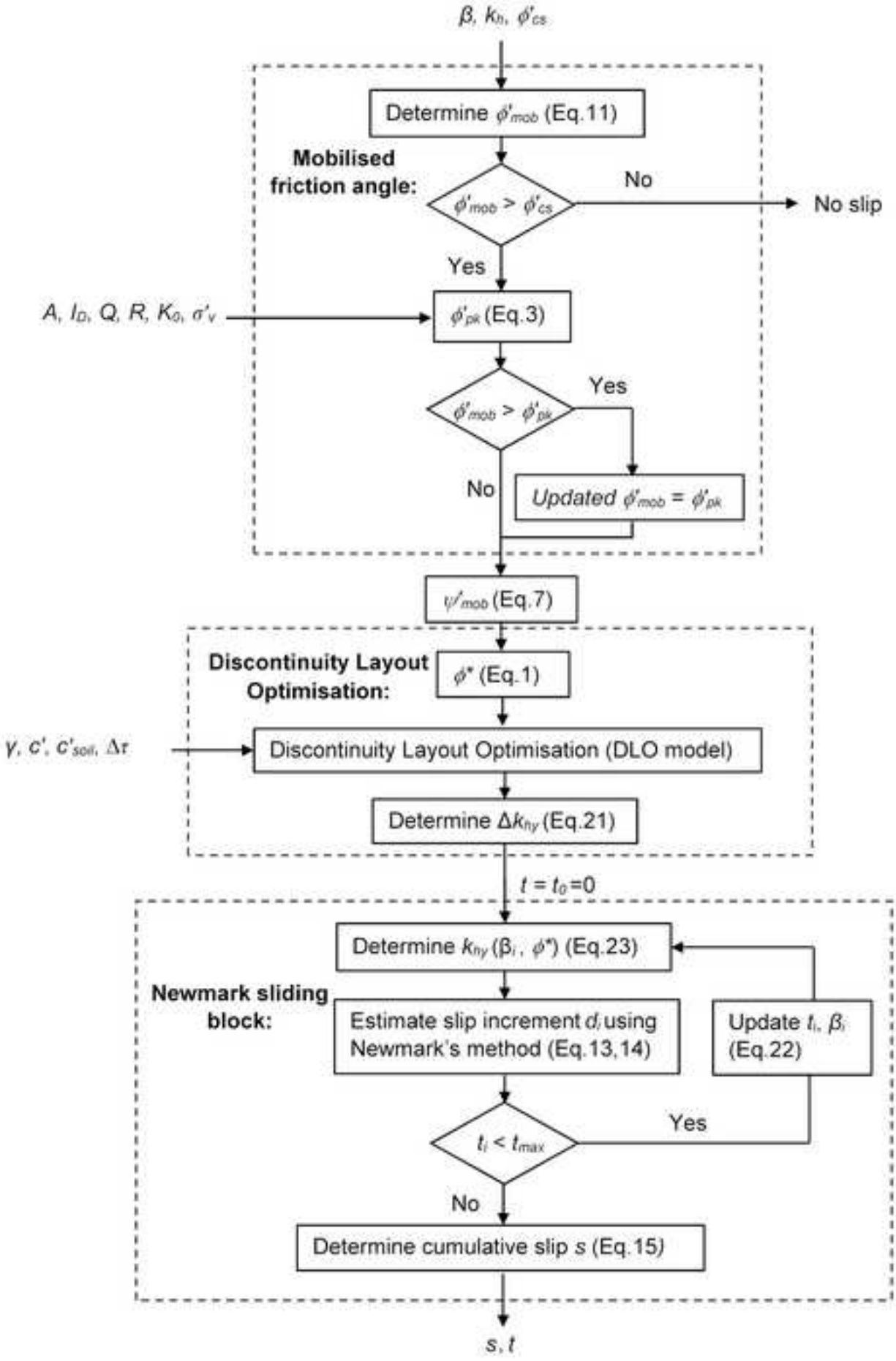

Figure 6

Click here to download high resolution image

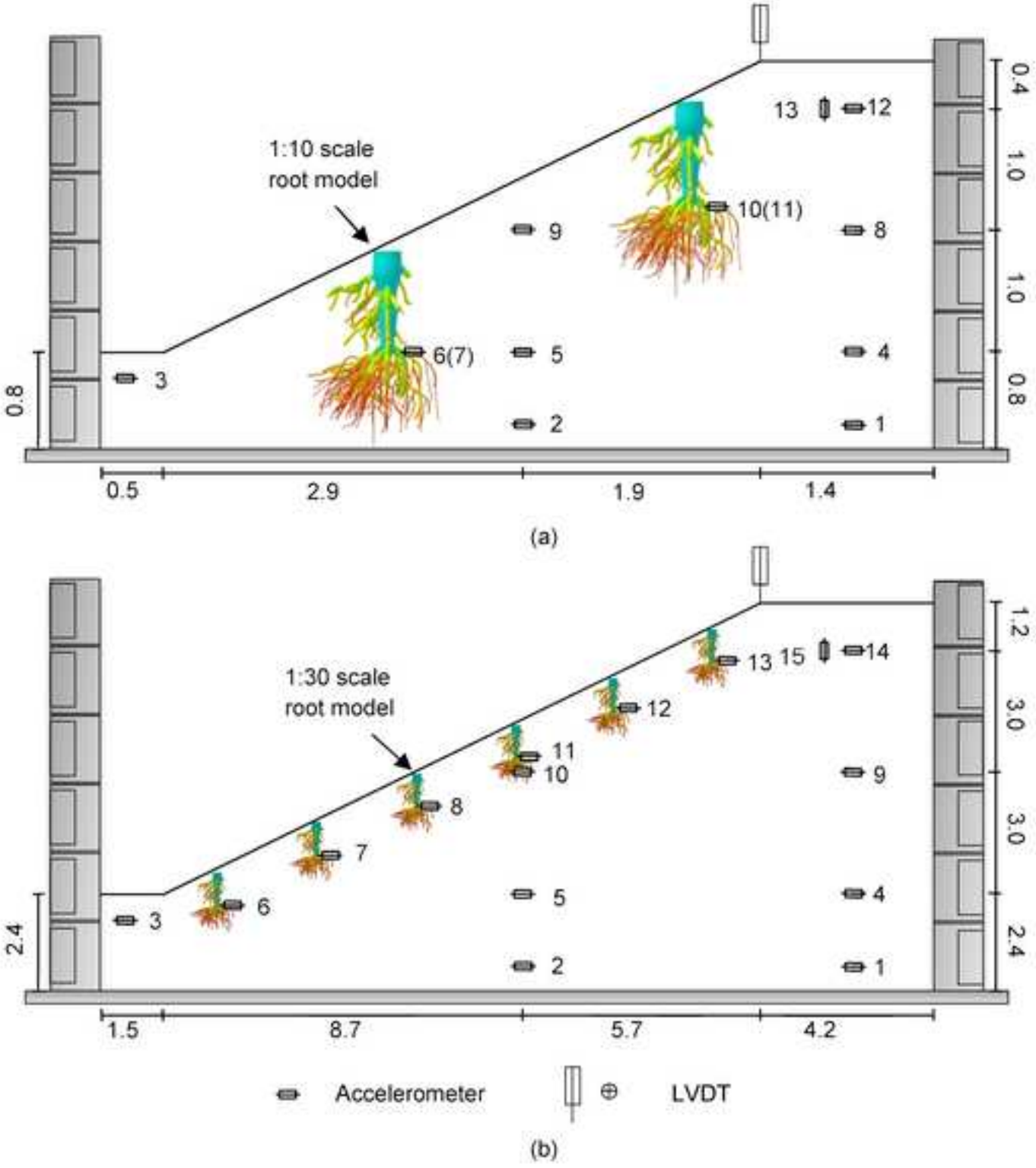

Figure 7
Click here to download high resolution image

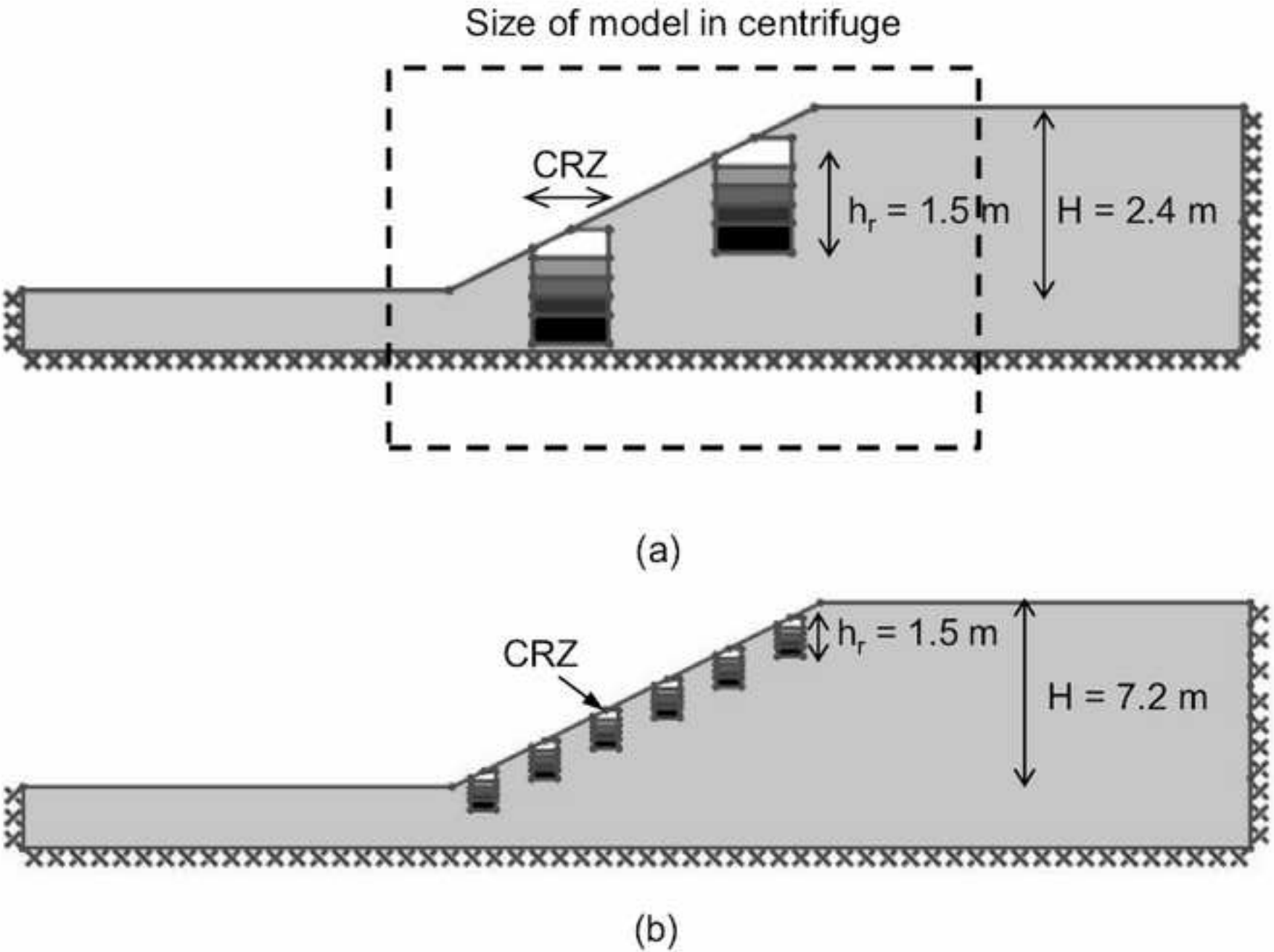

Figure 8

Click here to download high resolution image

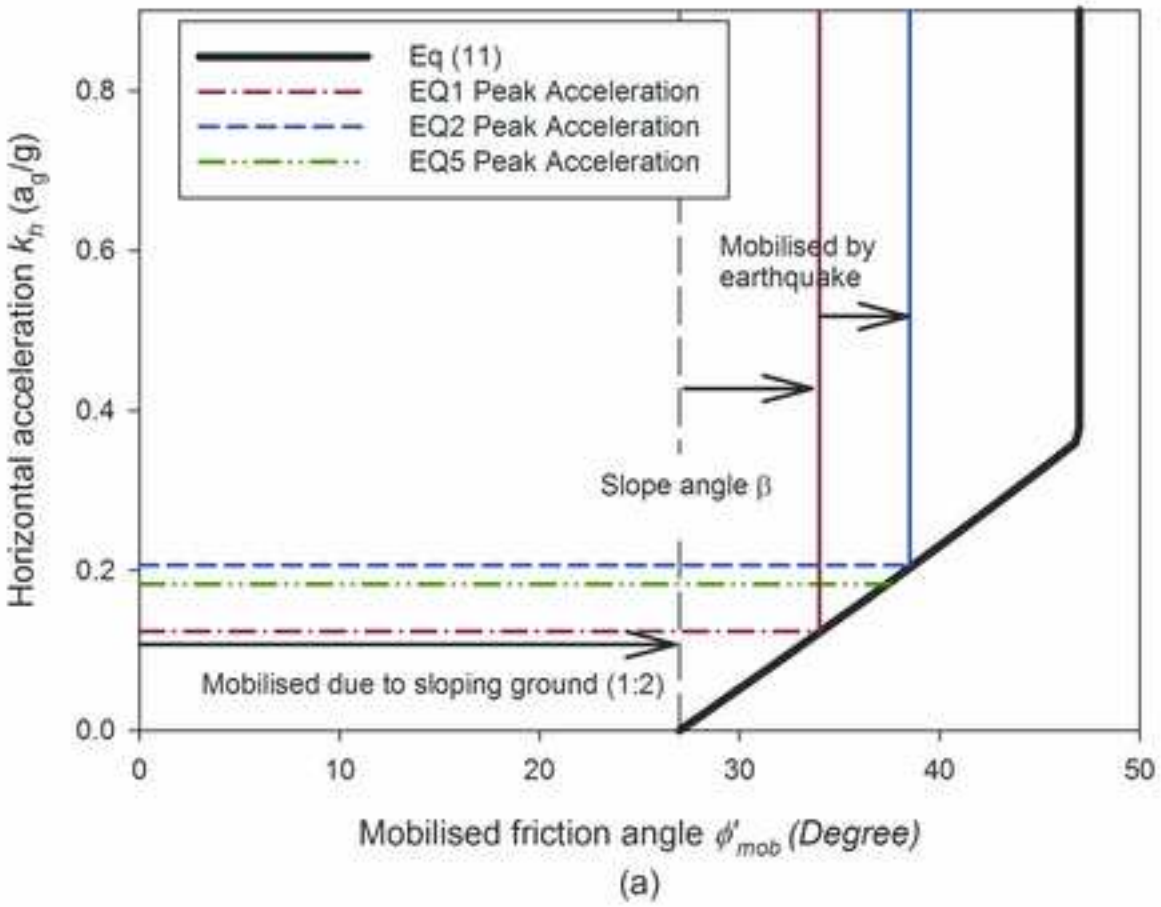

(a)

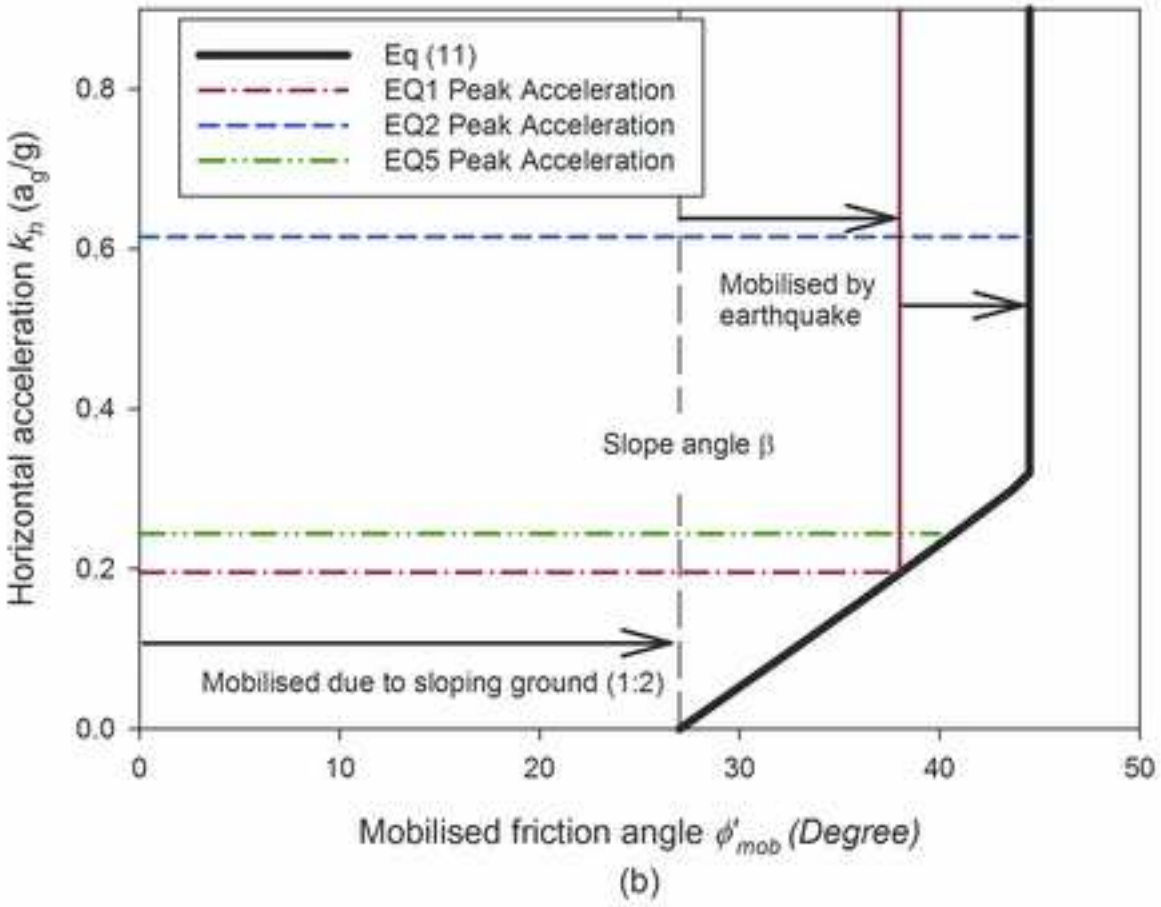

(b)

Figure 9
Click here to download high resolution image

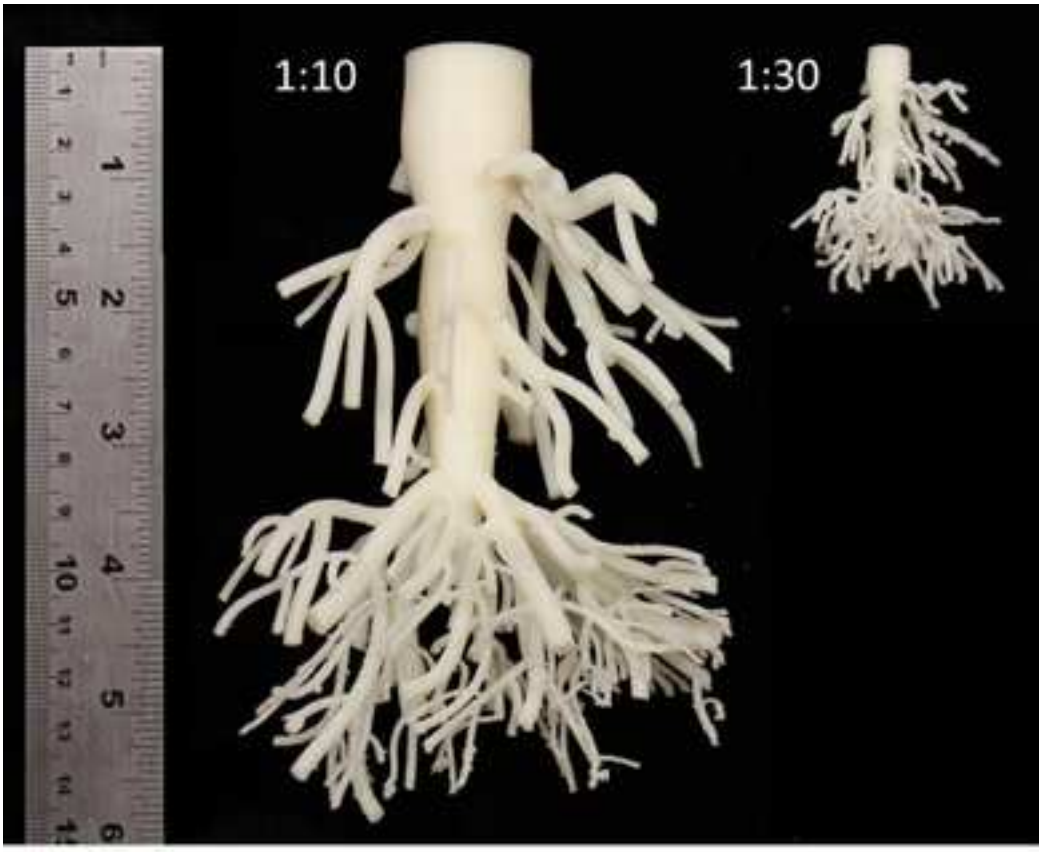

(a)

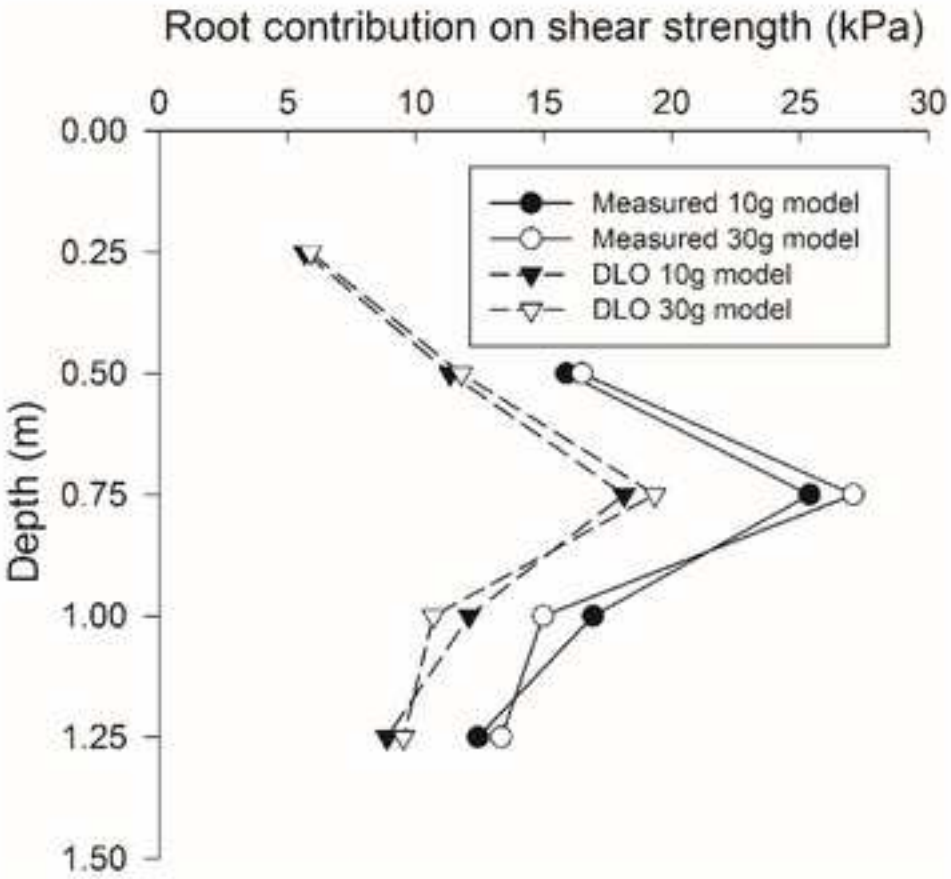

(b)

Figure 10
Click here to download high resolution image

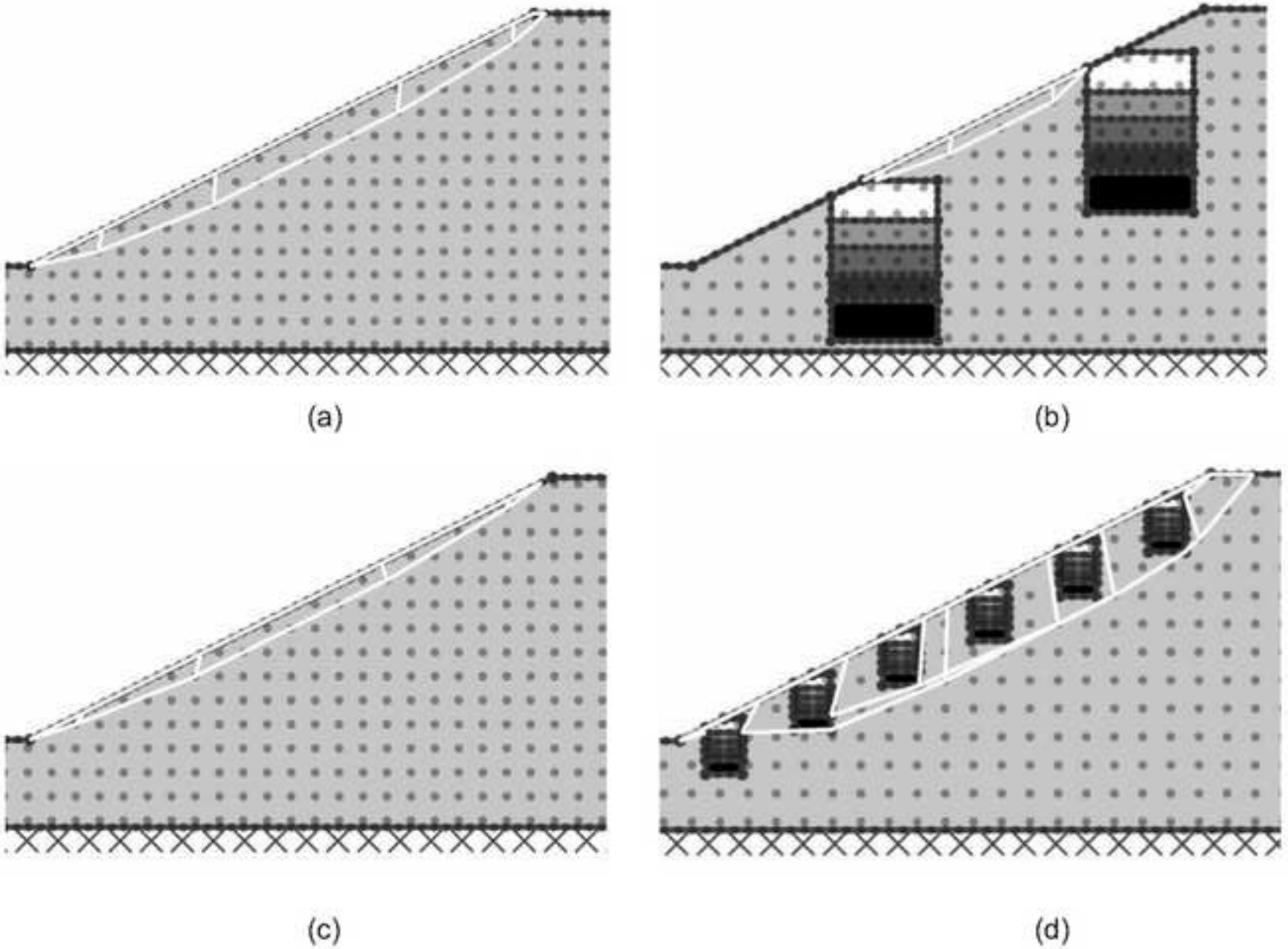

Figure 11

Click here to download high resolution image

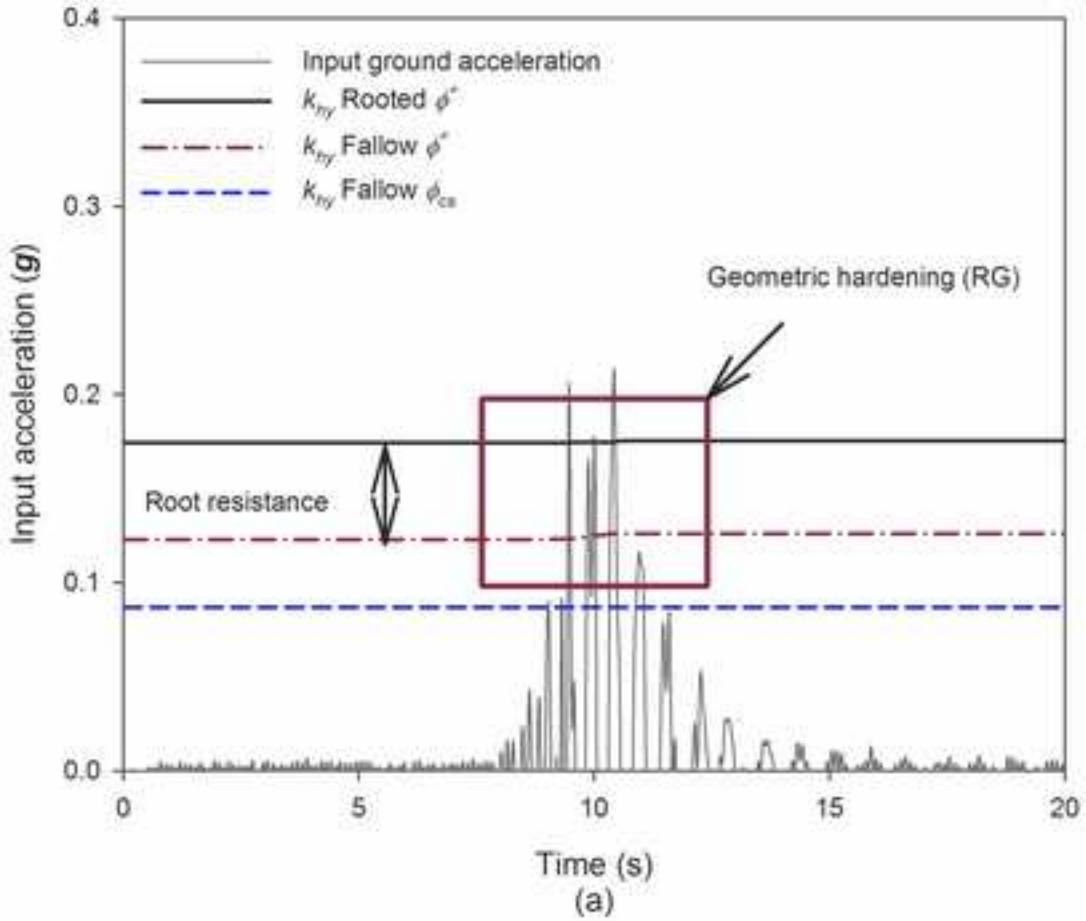

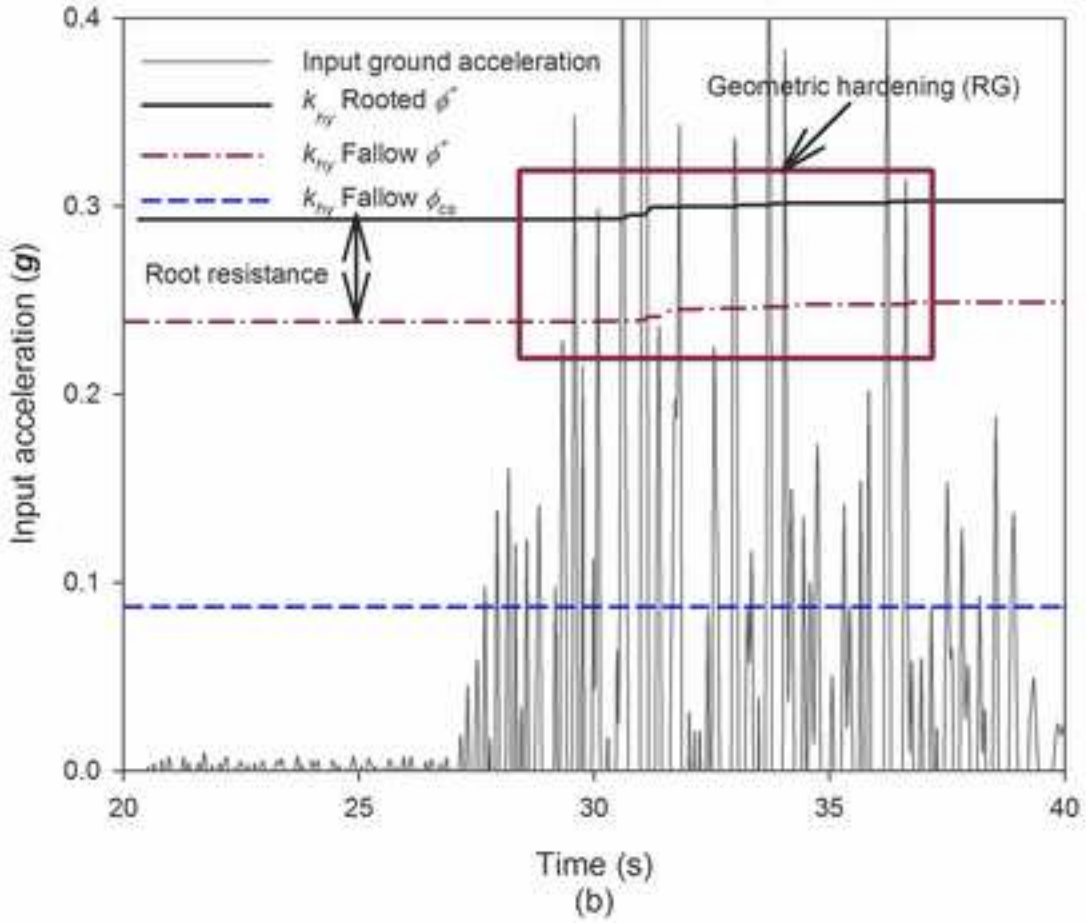

Figure 12

Click here to download high resolution image

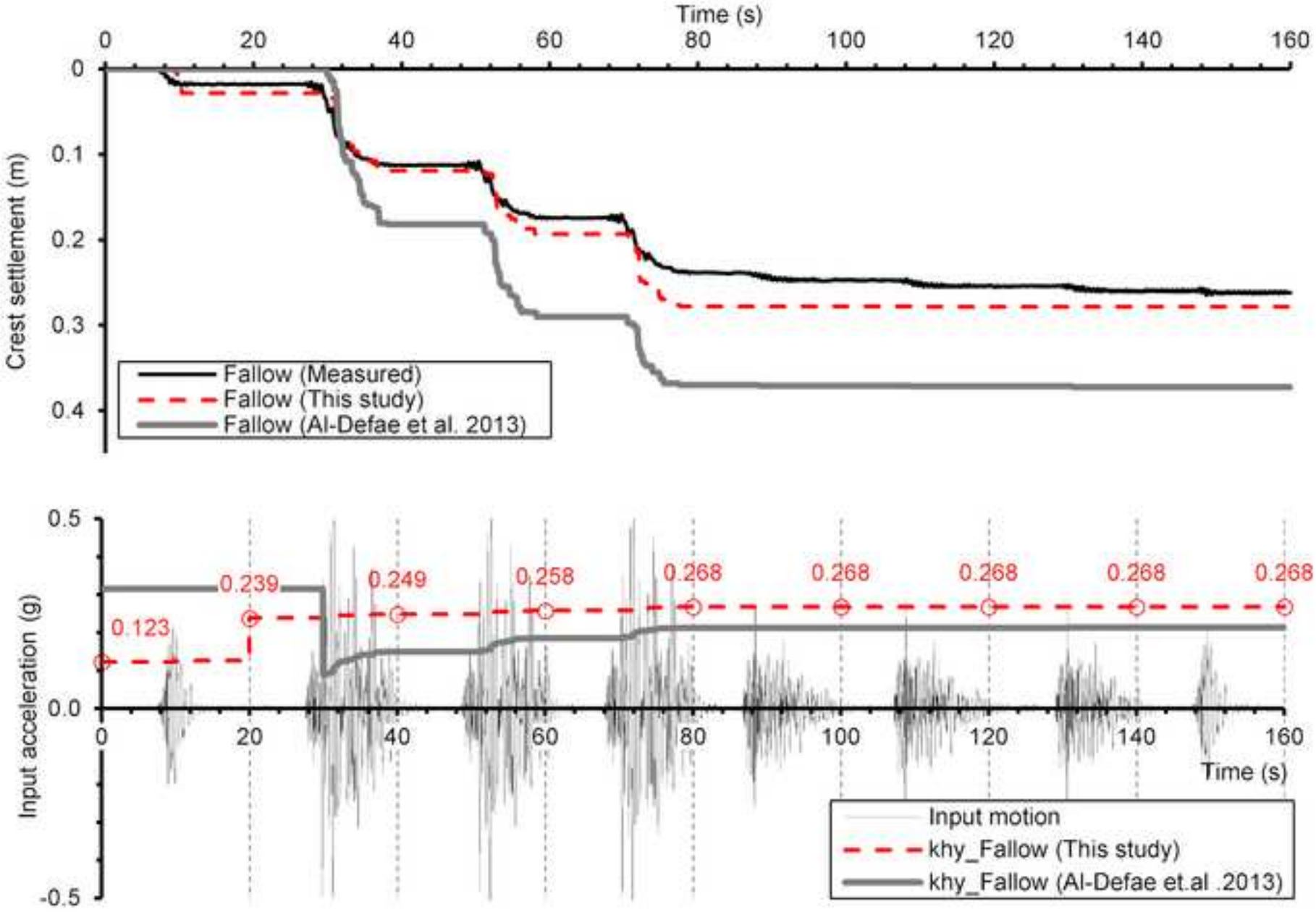

Figure 13

Click here to download high resolution image

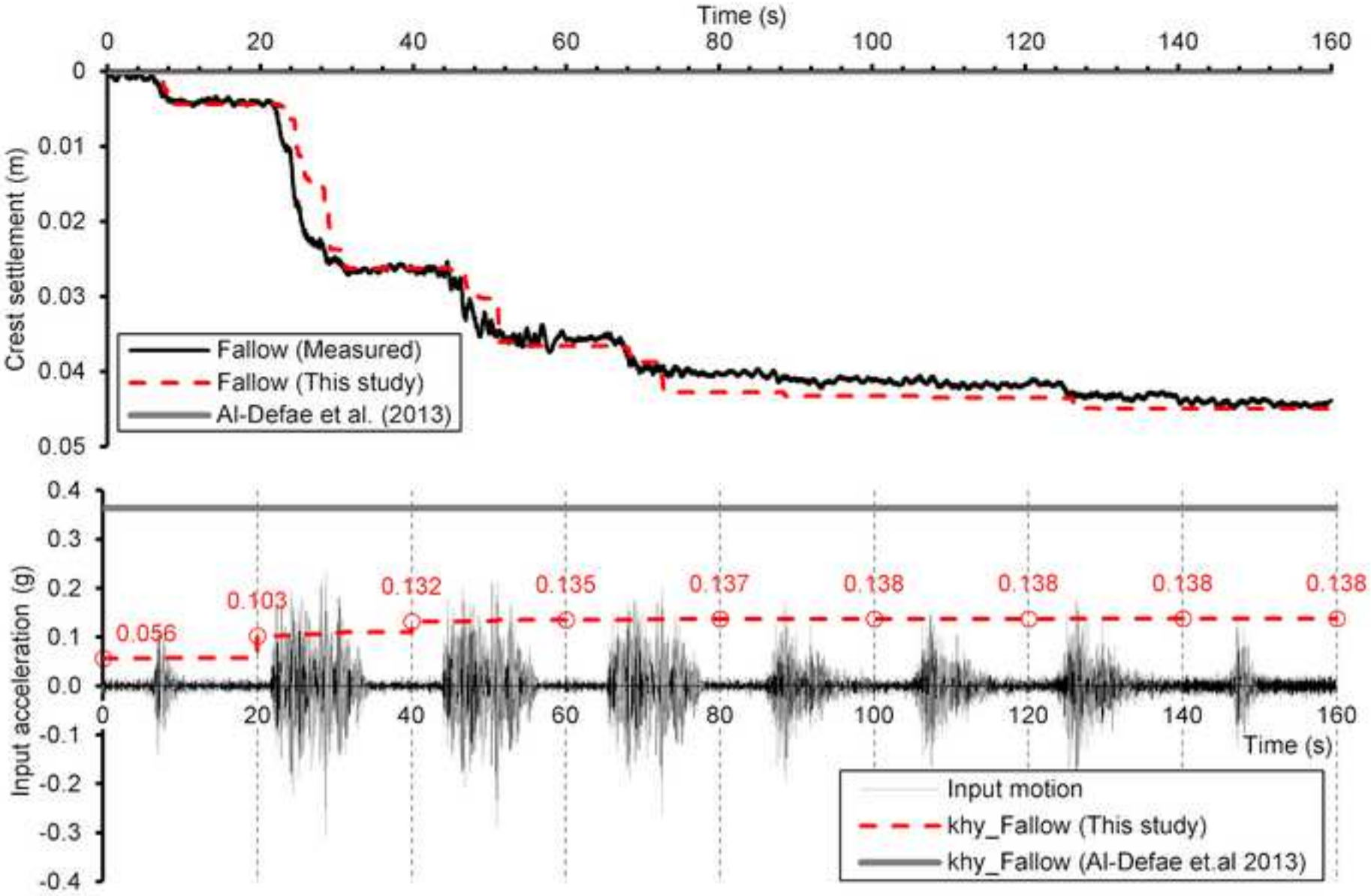

Figure 14

Click here to download high resolution image

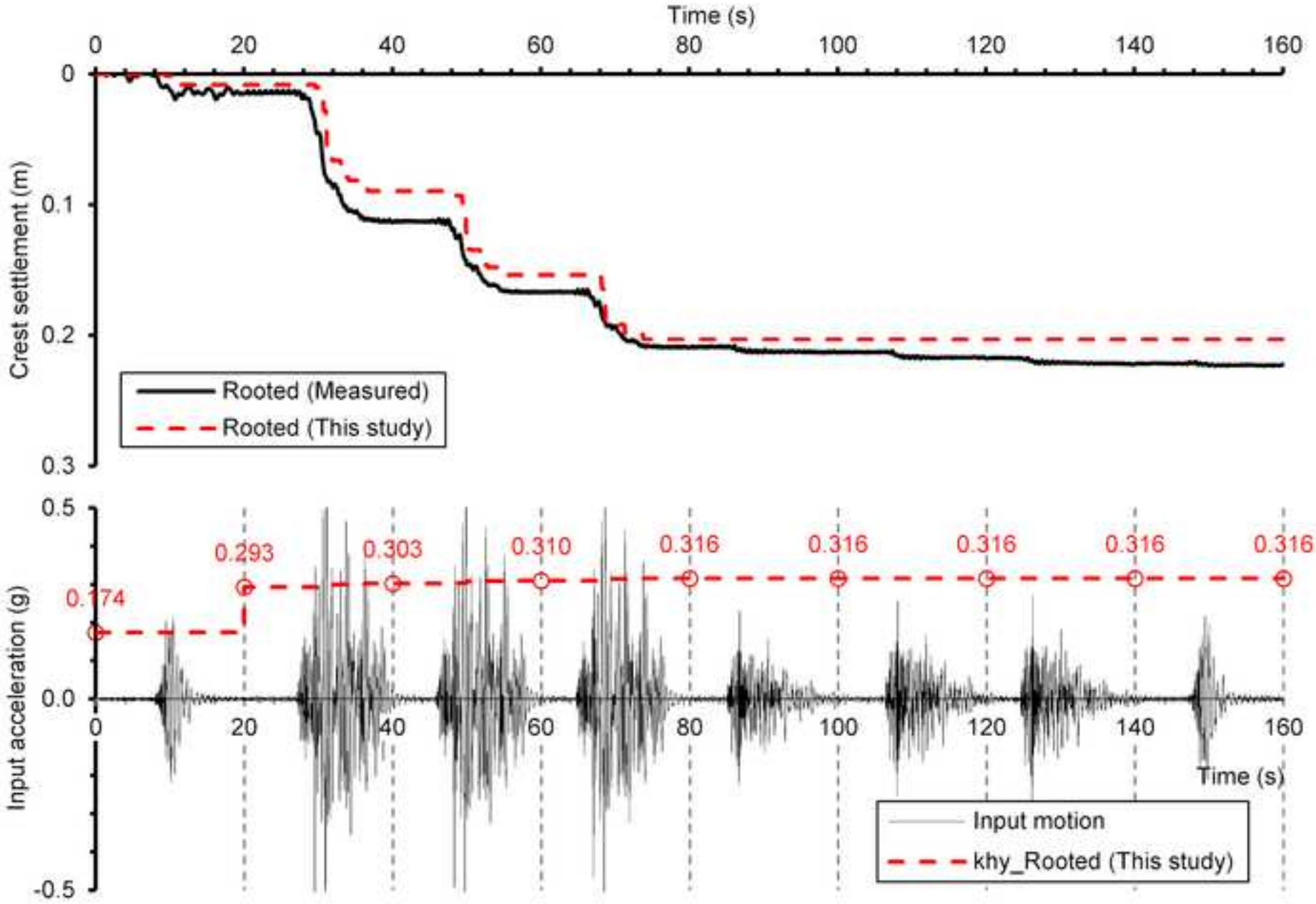

Figure 15

Click here to download high resolution image

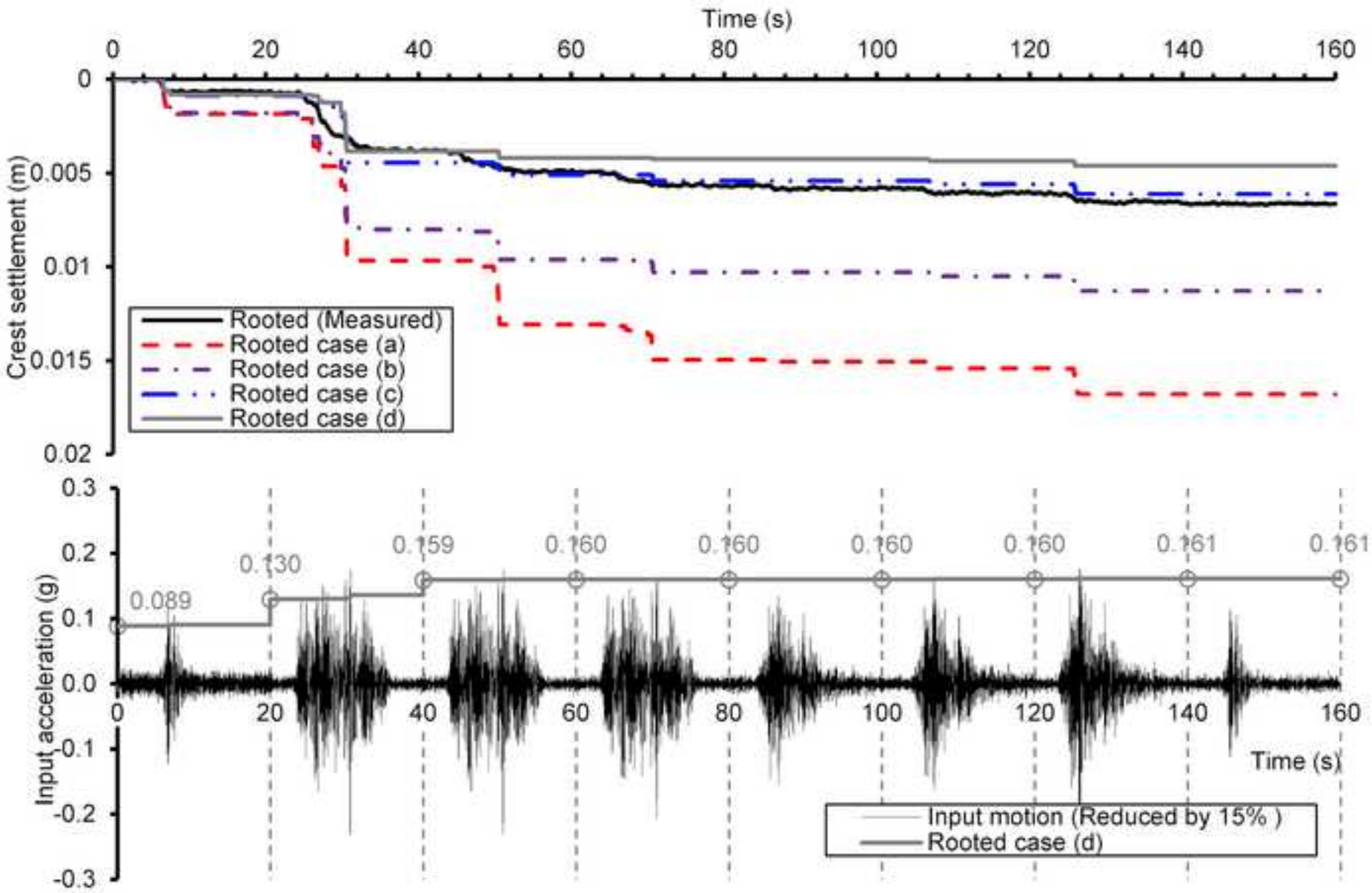

Figure 16
Click here to download high resolution image

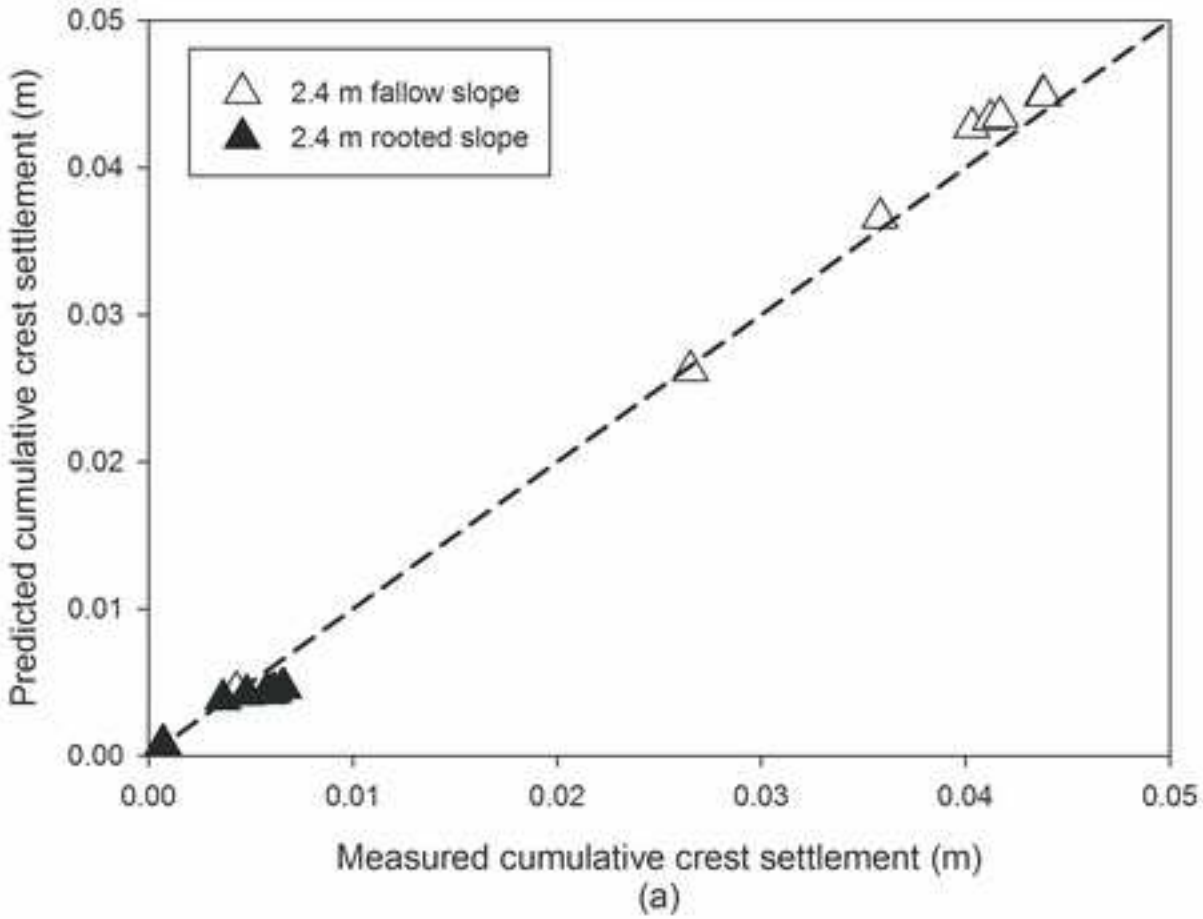

(a)

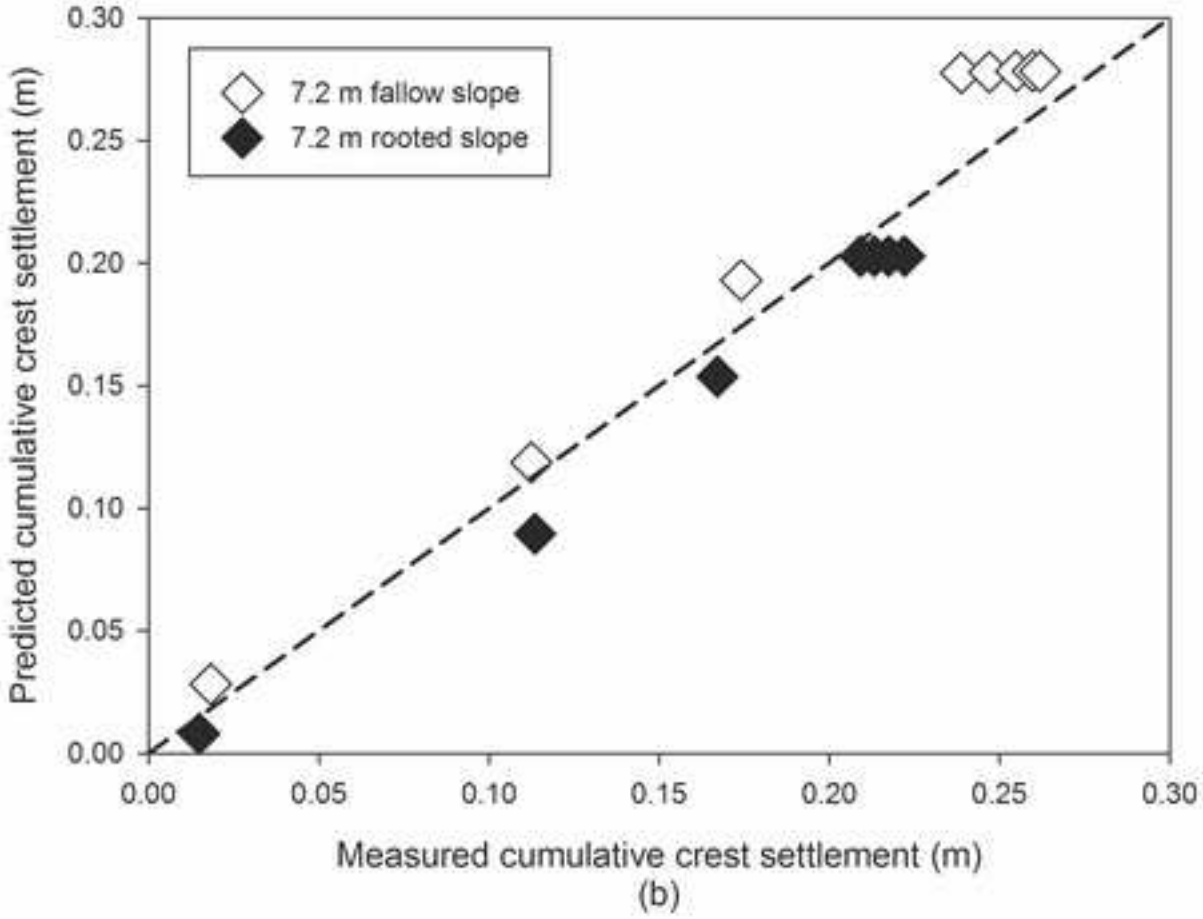

(b)

Figure 17
Click here to download high resolution image

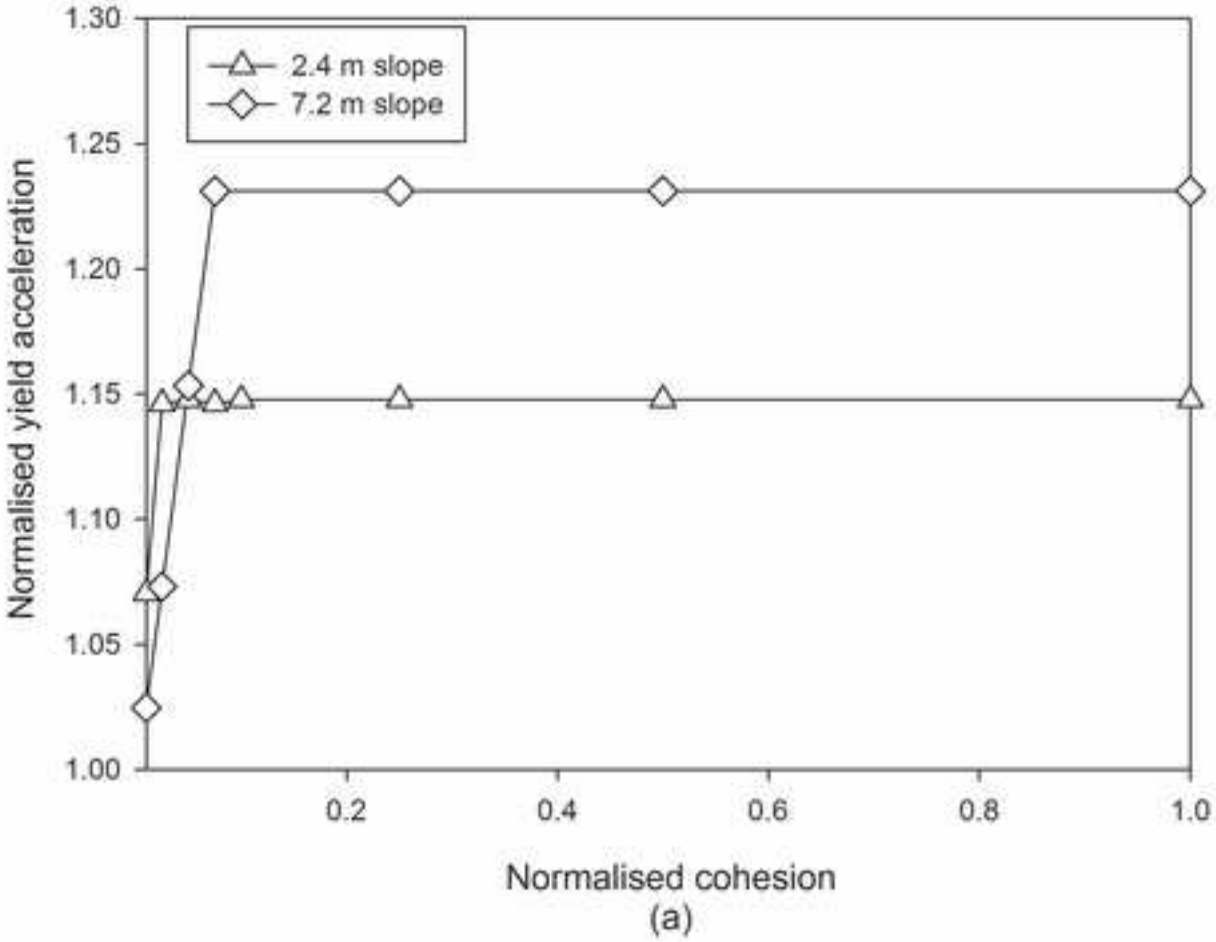

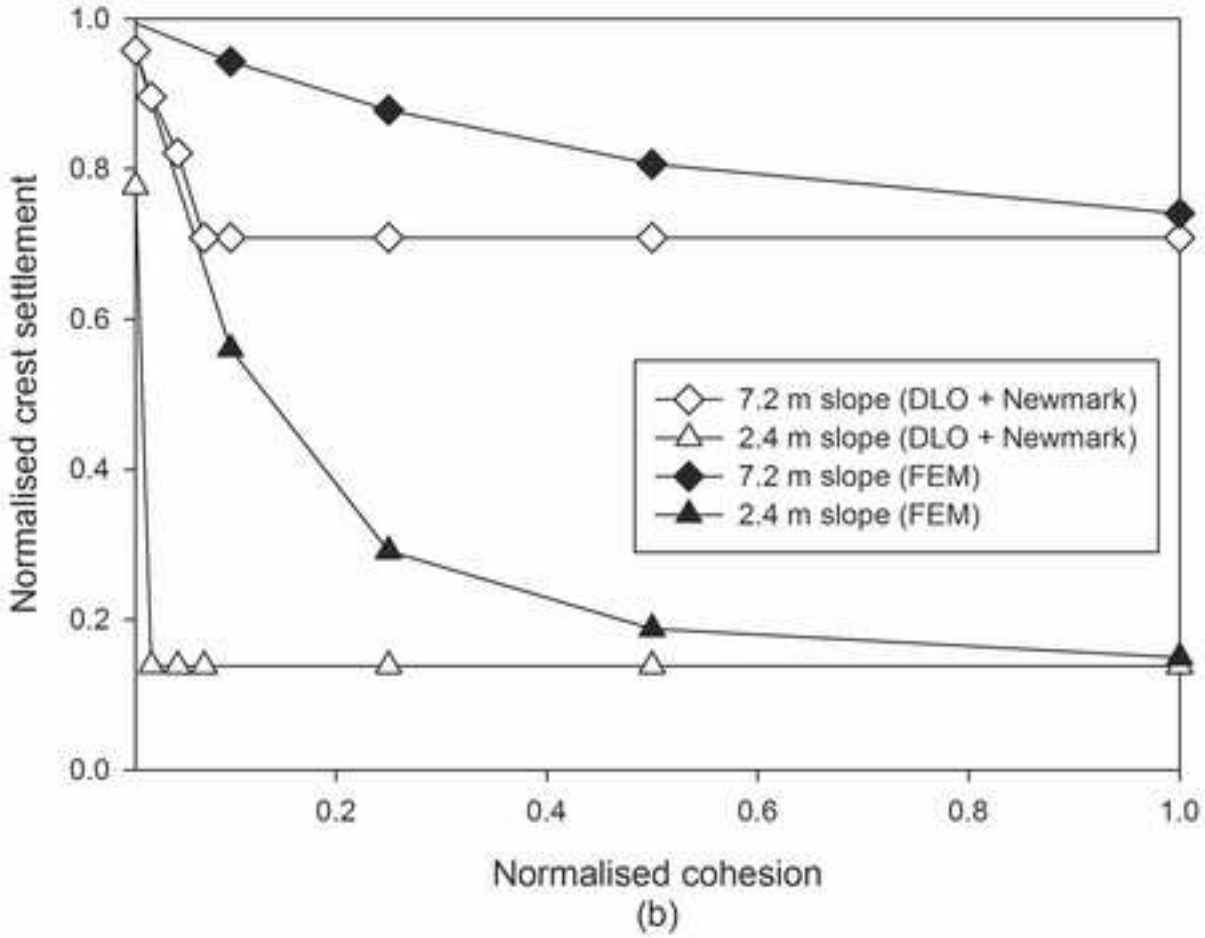

Figure 18
Click here to download high resolution image